NAVAL OCEAN SYSTEMS CENTER San Diego, California 92152-5000

Technical Report 1163
January 1987

Air Vehicle Detection by Using an Ensemble of Moving-Picture Images

Larry B. Stotts
Naval Ocean Systems Center

I. S. Reed
R. M. Gagliardi
Department of Electrical Engineering
and System Science,
University of Southern California

Approved for public release; distribution is unlimited.

87   6   23   020

NAVAL OCEAN SYSTEMS CENTER
San Diego, California 92152-5000

E. G. SCHWEIZER, CAPT, USN
Commander

R. M. HILLYER
Technical Director

ADMINISTRATIVE INFORMATION

ACKNOWLEDGMENTS

AD-A182161

REPORT DOCUMENTATION PAGE

1a REPORT SECURITY CLASSIFICATION	1b RESTRICTIVE MARKINGS
UNCLASSIFIED	

2a SECURITY CLASSIFICATION AUTHORITY	3 DISTRIBUTION/AVAILABILITY OF REPORT
2b DECLASSIFICATION/DOWNGRADING SCHEDULE	Approved for public release; distribution is unlimited.

4 PERFORMING ORGANIZATION REPORT NUMBER(S)	5 MONITORING ORGANIZATION REPORT NUMBER(S)
TR 1163	

6a NAME OF PERFORMING ORGANIZATION	6b OFFICE SYMBOL (If applicable)	7a NAME OF MONITORING ORGANIZATION
Naval Ocean Systems Center	Code 7402	

6c ADDRESS (City, State and ZIP Code)	7b ADDRESS (City, State and ZIP Code)
San Diego, CA 92152-5000	

8a NAME OF FUNDING/SPONSORING ORGANIZATION	8b OFFICE SYMBOL (If applicable)	9 PROCUREMENT INSTRUMENT IDENTIFICATION NUMBER

8c ADDRESS (City, State and ZIP Code)	10 SOURCE OF FUNDING NUMBERS			
	PROGRAM ELEMENT NO	PROJECT NO	TASK NO	AGENCY ACCESSION NO
	Local funding			DN306 233

11 TITLE (Include Security Classification)

Air Vehicle Detection by Using an Ensemble of Moving-Picture Images

12 PERSONAL AUTHOR(S)
L. B. Stotts, NOSC; I.S. Reed, R.M. Gagliardi, USC

13a TYPE OF REPORT	13b TIME COVERED	14 DATE OF REPORT (Year, Month, Day)	15 PAGE COUNT
Final	FROM _____ TO _____	January 1987	46

16 SUPPLEMENTARY NOTATION

17 COSATI CODES			18 SUBJECT TERMS (Continue on reverse if necessary and identify by block number)
FIELD	GROUP	SUB-GROUP	Air vehicle detection, target detection, moving-picture images, image sequencing, matched filtering, three-dimensional techniques, optics, signal processing, signal-to-noise ratios, complexity reduction

19 ABSTRACT (Continue on reverse if necessary and identify by block number)

Three-dimensional matched filtering of optical image sequences has recently been configured for moving-target detection applications. A method is described for reconfiguring this technique into a space-shift and time-delay-and-integrate match-filtering form to reduce signal-processing complexity and extent. Simulation studies were performed to verify the possible signal-to-noise ratio gains this approach offers, and to illustrate its potential as an MTI technique.

20 DISTRIBUTION/AVAILABILITY OF ABSTRACT	21 ABSTRACT SECURITY CLASSIFICATION
☒ UNCLASSIFIED/UNLIMITED ☐ SAME AS RPT ☐ DTIC USERS	UNCLASSIFIED

22a NAME OF RESPONSIBLE INDIVIDUAL	22b TELEPHONE (Include Area Code)	22c OFFICE SYMBOL
Larry B Stotts	(619) 225-2481	Code 7402

DD FORM 1473, 84 JAN

DD FORM 1473, 84 JAN

EXECUTIVE SUMMARY

PROBLEM

Examine three-dimensional matched filtering and show how it can be applied to accomplish target detection over sequences of observed scenes, which is an important extension of classical two-dimensional image processing. Provide examples to demonstrate and validate these results.

RESULTS

Three-dimensional filtering techniques can be easily modified to act as a space-shift, time-delay-and-integrate matched-filtering technique. Computer simulations verified the validity of this modification. The results demonstrate signal-to-noise ratio gains asymptotically growing by the filter integration time over those normally obtained by two-dimensional matched filtering of the individual frames in a sequence. The specific form of the output is ideally suited for moving-target indicator (MTI) applications, or can be used in conjunction with some other target-speed and detection-localizing algorithm.

CONTENTS

FIGURES

FIGURES (Continued)

iii

1.0 INTRODUCTION

A pressing problem in remote sensing is the detection of weak targets in highly spatially structured optical imagery. Such imagery can be generated by a scanning point detector or linear photodiode array, or by a staring mosaic photodiode array. Reviews of current image-processing trends have illustrated their utility for enhancing the inherent information content found in remotely sensed multispectral imagery [1-6]. Most of these techniques are generally suitable for feature extraction and or pattern-recognition applications, and as a consequence are not always helpful in the detection of small, weak targets. Other signal-processing techniques are used to provide target detection and localization [7].

When the target is moving with respect to the background, several signal-detection methods can be applied to the image pixel data to reduce the inherent background clutter in the imagery and enhance target detectability [7-12]. For example, the accepted approach for localizing targets in staring mosaic data sequences is to frequently bandpass the imagery by using either an analog or digital filter; e.g., frame-to-frame subtraction or a third-order transversal filter [7-9]. These techniques are known to produce excellent results provided the target is relatively strong. Otherwise, they must be used in concert with other signal-enhancing methods [7, 10-12].

Mohanty has shown that potential track trajectories of a weak point target can be assembled through exhaustive search of all possible trajectories in a given frame sequence [10]. Unfortunately, for a staring mosaic array of reasonable size, the number of possible trajectories to be searched can be large; hence it is an unattractive approach to target detection. Barniv used dynamic programming to reduce this approach to a more reasonable level through specific knowledge of potential speed windows and target shape [11].

A more robust track localization technique has been developed by Reed, Gagliardi, and Shao for detecting weak, moving targets in background clutter by using three-dimensional (3-D) matched filtering [12]. This method performs moving-target-signature matched filtering in the Fourier domain, with proper signal phasing automatically applied in order to "coherently" sum the target energy and reduce background noise. The result is a set of matched-filter peaks indicating detected pieces of track. Its strengths lie in its ability to operate on several potential target tracks simultaneously (independent of their respective space time origins) and to bring out partial as well as full tracks with enhanced signal-to-noise ratios often substantially in excess of what normally would be obtained from spatially filtering each individual frame separately. Its weakness is that this method requires knowledge of the moving target's temporal signature, an aspect not always known *a priori*. This apparent drawback can be compensated for, but at the cost of increasing the number of filter banks significantly to accommodate all possible temporal signature variations of each prospective target of interest.

To eliminate this last cost impact, the same filtering approach can be reconfigured as an ensemble moving-picture processor. Its specific form is of a space-shift and time-delay-and-integrate matched filter, and it retains much of the processing strength described above. However, its real impact is to reduce the number of filter banks to the level necessary for basic target velocity discrimination, and this can be reduced further by target parameter estimation by means of data fusion.*

---

*Kendall, W. B., Space Computer Corporation, private communication.

The intent of this report is to further examine three-dimensional matched filtering and to show how it can be applied to accomplish target detection over sequences of observed scenes, which is an important extension of classical two-dimensional image processing. Examples are given to demonstrate and validate these results.

2.0 ENSEMBLE MOVING-PICTURE PROCESSING

Reed, et al. [12], have shown that the optimum three-dimensional matched filter for a moving target is obtained by maximizing the received signal-to-noise ratio through linear filtering. Its specific form is

$$H(\underset{\sim}{k}:\omega) = \frac{A^*(\omega + \underset{\sim}{k} \cdot \underset{\sim}{v}) \, S_0(\underset{\sim}{k})}{\Phi_0(\underset{\sim}{k}:\omega) \, G(\underset{\sim}{k})} \tag{1}$$

where

$$A(\omega) = \iint\limits_{-\infty}^{+\infty} a(t) \exp\{-i\omega t\} dt \tag{2}$$

$$S_0(\underset{\sim}{k}) = \int\limits_{-\infty}^{+\infty} s_0(\underset{\sim}{r}) \exp\{-i\underset{\sim}{k} \cdot \underset{\sim}{r}\} d^2 r \tag{3}$$

$$\Phi_0(\underset{\sim}{k}:\omega) = \iiint\limits_{-\infty}^{+\infty} \phi_0(\underset{\sim}{r}:t) \exp\{-i\underset{\sim}{k} \cdot \underset{\sim}{r} - i\omega t\} d^2 r \, dt \tag{4}$$

and

$$G(\underset{\sim}{k}) = \iint\limits_{-\infty}^{+\infty} |h(\underset{\sim}{r})|^2 \exp\{-i\underset{\sim}{k} \cdot \underset{\sim}{r}\} d^2 r \tag{5}$$

where the authors have assumed a moving target of spatial profile $s_0(r)$ and temporal intensity function $a(t)$ traversing a certain portion of terrain with velocity $\underset{\sim}{v}$. This terrain is assumed to possess colored Gaussian intensity statistics with autocorrelation $\phi_0(r:t)$. The entire scenario is imaged in an optical system with point-spread function $|h(r)|^2$ onto a large high-density, high-speed photodiode array. The appendix contains a detailed derivation of the optimum filter $H(\underset{\sim}{k}:\omega)$. The resulting data sequence is assumed after sampling to be quasi-stationary in intensity, space, and time, and forms a continuous "moving picture," which will be image processed to yield the existence of the moving target. On the assumption that the signal is additive to the noise, the two possible output sequences are

$$y(\underset{\sim}{r}:t) = n_0(\underset{\sim}{r}:t) \tag{6a}$$

and

$$y(\underset{\sim}{r}:t) = n_0(\underset{\sim}{r}:t) + s(\underset{\sim}{r}:t) \tag{6b}$$

2

with the particular choice depending on whether the target is absent or present, respectively. Here $n_0(\underline{r};t)$ and $s(\underline{r};t)$ are the received background and target intensity distributions, respectively (see appendix A).

In general, the exact form of the target temporal intensity function $a(t)$ is not known beforehand. This implies that the size of the matched-filter bank will be quite large, since it must encompass all possible targets, shapes, velocity windows, track orientations, and, now, intensity functions. Such additional complexity would generally make this approach undesirable. However, if the above three-dimensional matched-filter approach is restructured as a space-shift and time-delay-and-integrate matched filter, significant target signal-to-noise ratio gains are still achievable, and with reduced processing complexity. In this technique, $a(t)$ is replaced as the temporal intensity variation by a processing window function for simultaneously interacting the various frame groups within the sequence. The simplest form for $a(t)$ is a rectangular time function of width, T_1 seconds, centered about $t = 0$. Mathematically, this is expressed as

$$a(t) = \text{rect } [t] = \begin{cases} 1 & : \ |t| \leqslant T_1/2 \\ 0 & : \ \text{otherwise} \ . \end{cases}$$

As will be shown, the input sequence must be greater than or equal to T_1 so that this technique will yield optimal results. The potential signal-to-noise ratio in this case is derived below. For simplicity and without loss in generality, let $E[n_0(r;t)] = 0$. Also, let the noise spectrum be white Gaussian and the point-spread function of the optical system $|h(\underline{r})|^2$ equal $\delta(\underline{r})$.

For an image sequence of long duration, the input signal intensity has a Fourier transform of the form

$$S(\underline{k}:\omega) = T_0 \text{ sinc } [(\omega + \underline{k} \cdot \underline{v}) T_0/2\pi] \ S_0(\underline{k}) \ e^{-i\underline{k} \cdot \underline{r}_0} \tag{7}$$

where

$T_0 \equiv$ frame sequence length $(\geqslant T_1) = MT_0'$

$T_0' \equiv$ time between frames, and

$$\text{sinc } [\sigma] = \frac{\text{sinc } (\pi.\sigma)}{\pi\sigma} \ . \tag{8}$$

Figure 1 illustrates a target moving across a fixed scene in $M = T_0 \ T_0$ frames of a sufficiently large sequence of images. Using equation 1 with a rectangular-window signal function, the optimum three-dimensional filter becomes

$$H (\underline{k}:\omega) = T_1 \text{ sinc } [(\omega + \underline{k} \cdot \underline{v}) T_1/2\pi] \ \frac{S_0^*(\underline{k})}{N_0} \tag{9}$$

for a white-Gaussian background-clutter target-detection scenario. This implies that the output image has a mean level at the target position equal to
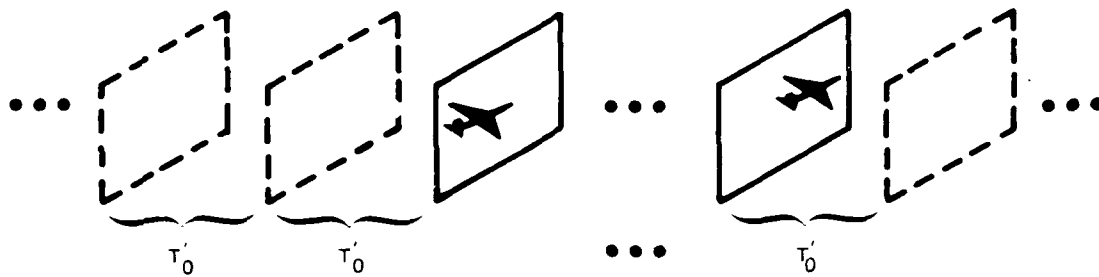
FINITE DATA SEQUENCE:

Figure 1. Example image set containing a moving target transvering a fixed scene during a finite portion of a countably infinite data sequence.

$$E\{y(\underset{\sim}{r};t)\} = \frac{1}{(2\pi)^3} \int\!\!\!\int\!\!\!\int_{-\infty}^{+\infty} H(\underset{\sim}{k};\omega)\, S(\underset{\sim}{k};\omega)\, \exp\{i\underset{\sim}{k} \cdot \underset{\sim}{r} + i\omega t\}\, d^2k\, d\omega$$

$$= \frac{T_0 T_1}{(2\pi)^3} \int\!\!\!\int\!\!\!\int_{-\infty}^{+\infty} \frac{|S_0(\underset{\sim}{k})|^2}{N_0}\, \text{sinc}\,[(\omega + \underset{\sim}{k} \cdot \underset{\sim}{\nu})\, T_0/2\pi] \tag{10}$$

$$\times\, \text{sinc}\,[(\omega + \underset{\sim}{k} \cdot \underset{\sim}{\nu})\, T_1/2\pi]\, \exp\{i\underset{\sim}{k} \cdot (\underset{\sim}{r} - \underset{\sim}{r}_0) + i\omega t\}\, d^2k\, d\omega$$

$$= \int\!\!\!\int_{-\infty}^{+\infty} \frac{S_0(\underset{\sim}{r}' - \underset{\sim}{r} + \underset{\sim}{r}_0 + \underset{\sim}{\nu}t)\, S_0^*(\underset{\sim}{r}')}{N_0}\, d^2r' \int_{-\infty}^{+\infty} \text{rect}\!\left[\frac{t'}{T_0}\right]\!\text{rect}\!\left[\frac{t \cdot t'}{T_1}\right]\! dt' \tag{11}$$

$$= B(t) \int\!\!\!\int_{-\infty}^{+\infty} \frac{S_0(\underset{\sim}{r}' - \underset{\sim}{r} + \underset{\sim}{r}_0 + \underset{\sim}{\nu}t)\, S_0^*(\underset{\sim}{r}')}{N_0}\, d^2r' \tag{12}$$

where

$$B(t) = \begin{cases} 0 & ; & |t| > |T_0/2 + T_1/2| \\ t + T_0/2 + T_1/2 & ; & -T_0/2 - T_1/2 \leqslant t < -T_0/2 + T_1/2 \\ T_1 & ; & |t| \leqslant |T_0/2 - T_1/2| \\ T_0/2 + T_1/2 - t & ; & T_0/2 - T_1/2 \leqslant t < T_0/2 + T_1/2 \end{cases} \tag{13}$$

From equation 13, it is apparent that the matched-filter peak(s) occur within the central portion of the second image sequence of time length T_0. Normally, this peak(s) would be expected to appear towards the end of the data sequence. However, the central processing peak approach was chosen out of a desire for symmetry in the processed output and will be

4

retained for the remainder of this report. Both output approaches are correct, but those readers desiring the classical result need only multiply equation 9 by the appropriate phase term to shift the filter peak to the sequence end.

The image variance is given by

$$\text{VAR}\,[y(\underset{\sim}{r};t)] = \frac{N_0}{(2\pi)^3} \iiint\limits_{-\infty}^{+\infty} |H(\underset{\sim}{k};\omega)|^2 \, d^2k\,d\omega \tag{14}$$

$$= \frac{1}{(2\pi)^3} \iint\limits_{-\infty}^{+\infty} \frac{|S_0(\underset{\sim}{k})|^2}{N_0} \, d^2k \, (T_1)^2 \int\limits_{-\infty}^{+\infty} \text{sinc}^2\left[\frac{\omega'T_1}{2\pi}\right] d\omega' \tag{15}$$

$$= \frac{1}{2\pi} \iint\limits_{-\infty}^{+\infty} \frac{|S_0(\underset{\sim}{r}')|^2}{N_0} \, d^2r'(4/\pi) \int\limits_{0}^{\infty} \frac{\sin^2\left(\frac{\omega'T_1}{2}\right)}{(\omega')^2} d^2\omega' \tag{16}$$

$$= T_1 \iint\limits_{-\infty}^{+\infty} \frac{|S_0(\underset{\sim}{r}')|^2}{N_0} \, d^2r' \; . \tag{17}$$

Thus the resulting signal-to-noise ratio can be written as

$$\text{SNR} = \frac{(E\{y(\underset{\sim}{r};t)\})^2}{\text{VAR}\,[y(\underset{\sim}{r};t)]} \tag{18}$$

$$= \frac{B^2(t)\left[\iint\limits_{-\infty}^{+\infty} \frac{S_0(\underset{\sim}{r}' - \underset{\sim}{r} + \underset{\sim}{r}_0 + \underset{\sim}{\nu}t)\,S_0^*(\underset{\sim}{r}')}{N_0} \, d^2r'\right]^2}{T_1 \iint\limits_{-\infty}^{+\infty} \frac{|S_0(\underset{\sim}{r}'')|^2}{N_0} \, d^2r''} \tag{19}$$

$$\rightarrow T_1 \iint\limits_{-\infty}^{+\infty} \frac{|S_0(\underset{\sim}{r}')|^2}{N_0} \, d^2r' \tag{20}$$

at its peak location. It is apparent from equation 20 that three-dimensional matched filtering yields a peak signal-to-noise ratio increase over two-dimensional matched filtering by a factor of T_1, the temporal width of the rectangular time filter. Clearly, this gain can be significant for most reasonable integration times. However, it should be emphasized that these results hold only for constant target intensity. Adjustments in the required SNR margin should be made for intensity variations such as scintillation and fading of the target, which might occur during the filter integration time. In the following section, a sequence of computer-generated images with a modeled airplane moving across the frames is used to verify these results.

5

3.0 ENSEMBLE MOVING-PICTURE PROCESSING OF SIMULATED DATA

To test the above theoretical formulation, three groups of 30 sample sets were created. Each sample set consisted of 19 white Gaussian images, with a modeled airplane propagating across each of them. The random numbers used in each group of each set were independently obtained from a mathematical procedure suggested by Dillard [13]. Each group contained zero mean image sequences with an average noise clutter of 10.0. The three groups are distinguished by having target signatures with single-pixel signal-to-noise ratios of 6 dB, 0 dB, and –6 dB, respectively. Here we define the single-pixel signal-to-noise ratio to be

$$SNR_i = \frac{[\overline{S_0} - \overline{B}]^2}{\sigma^2} \tag{21}$$

with $\overline{S_0} \equiv$ intensity value of the target within one pixel

$\overline{B} \equiv$ mean background intensity level
$= 0.0$ for this simulation

and $\sigma \equiv$ Standard deviation of the background clutter
$[= 10.0$ for this simulation].

Figure 2 illustrates an example frame of data and the spatial profile of the simulation target. In this figure, the spatial dimensions of the image are 23×23 pixels and the signal-to-noise ratio at one target pixel is 23.5 dB. Figure 3 shows the same frame as in figure 2, except that the target signal-to-noise ratio is 0 dB. The speed of the target was set at a uniform 1 pixel per frame. Specific matched filters were generated by using equation 1 for each image sequence for the following integration time windows: T = 1, 3, 4, 9, 11, 15, and 19. Each image and each sequence were zero-filled to yield $45 \times 45 \times 45$ arrays to minimize image wraparound when processed by using the discrete, finite-interval Fourier transform. Figures 4, 5, and 6 plot the expected signal-to-noise ratio given in equation 19 for the matched-filter peak as a function of frame number for initial single-target-pixel signal-to-noise ratios (SNR) equal to 6 dB, 0 dB, and –6 dB, respectively. For these calculations, the peak signal-to-noise ratio can be written as

$$SNR_p = 10 \log_{10} T_1 + 10 \log_{10} (15) + SNR_i \text{ (dB)} \tag{22a}$$

$$= 10 \log_{10} (T_1) + 11.76 \text{ dB} + SNR_i \tag{22b}$$

in decibels. The first term represents the processing gain from temporal matched filtering, the second represents the gain from spatial matched filtering (equal to the number of independent samples composing the target), and the third term is the inherent signal-to-noise ratio of the target in this background clutter. These last two terms comprise the expected peak signal-to-noise ratio obtainable from two-dimensional matched filtering. Using equation 22b, the linear increase of signal-to-noise ratio with observation time can clearly be seen in these three figures.

INITIAL TARGET PROFILE
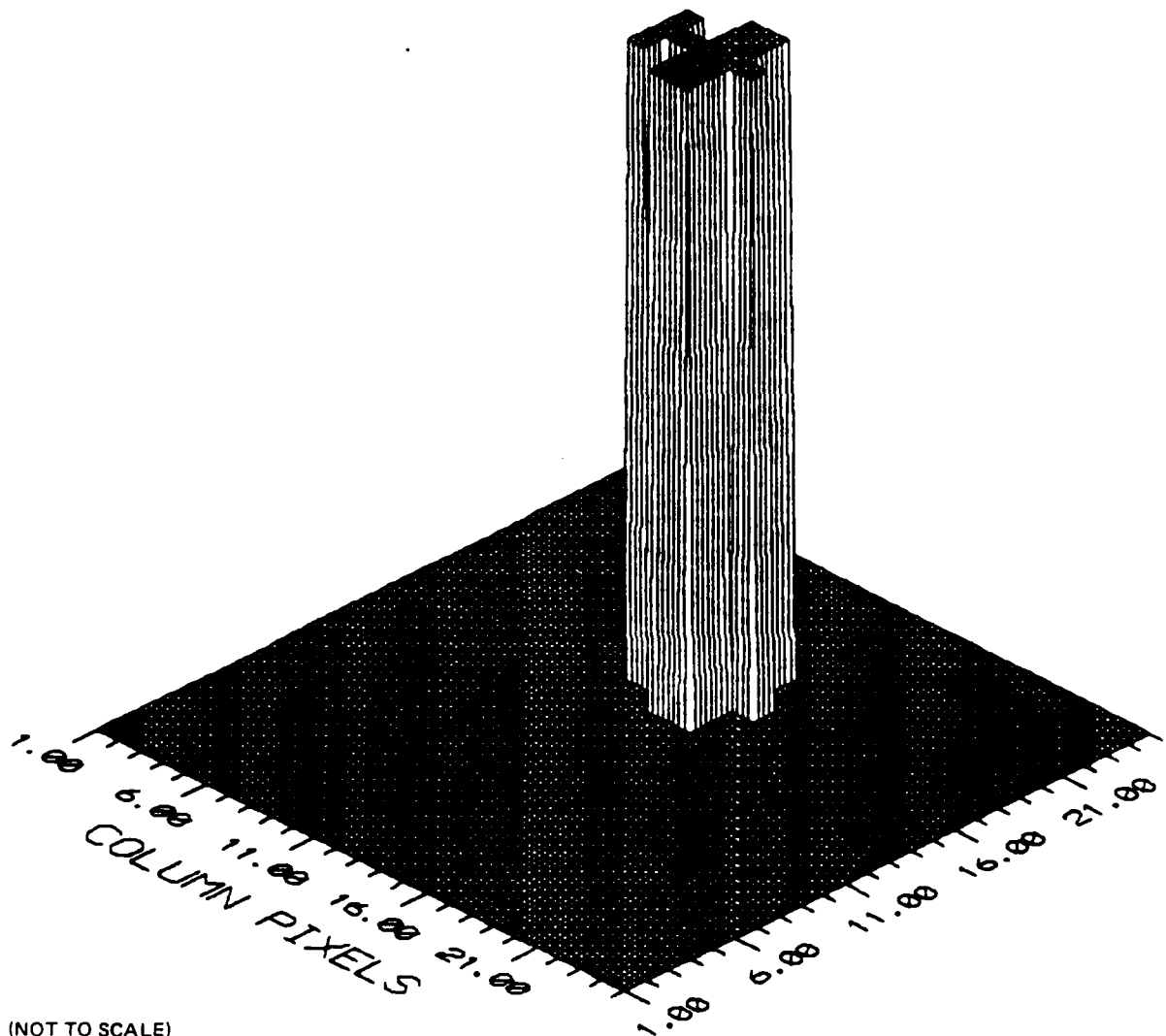
(NOT TO SCALE)

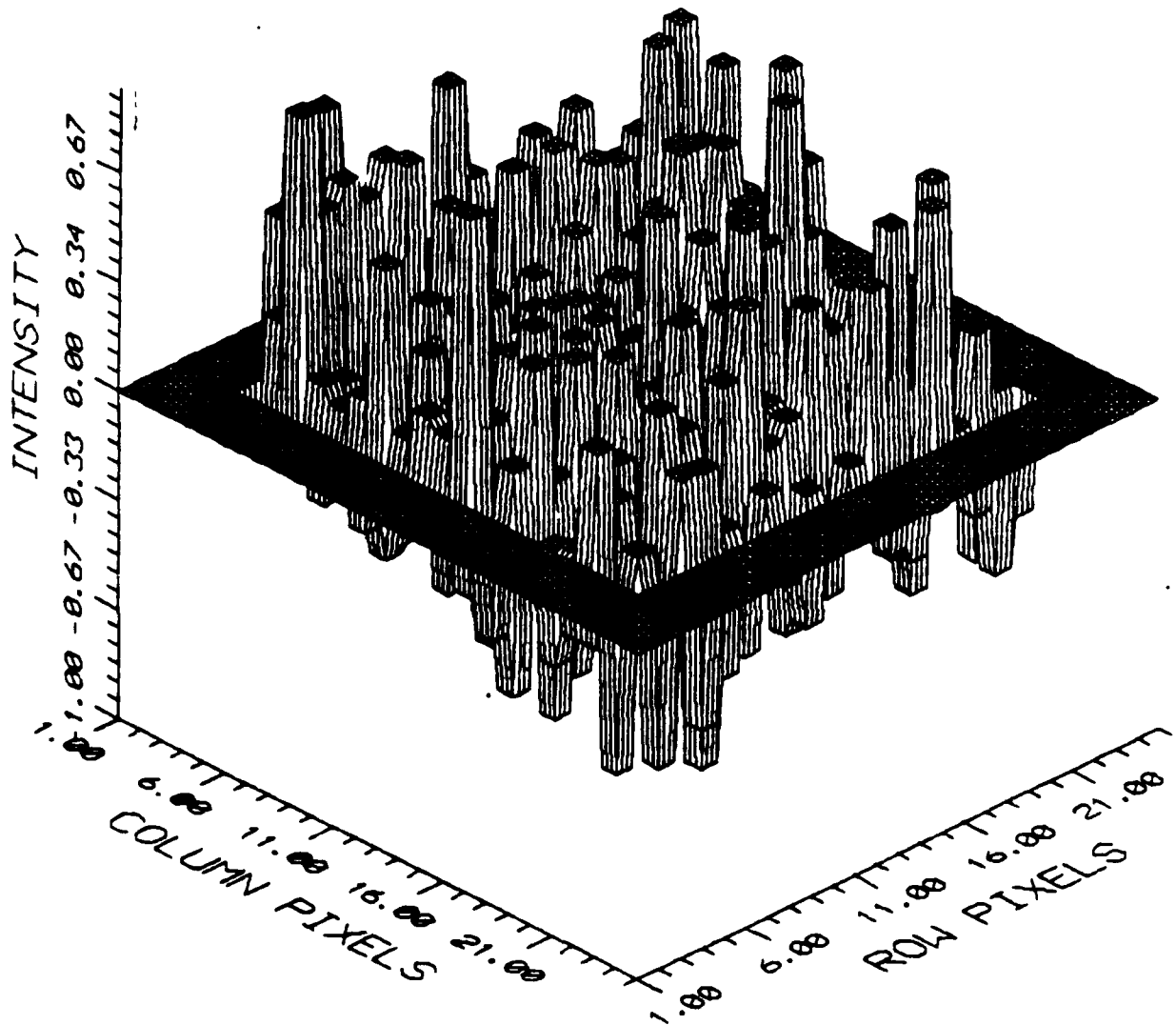Figure 2. Spatial profile of simulation target.

0 dB SIGNAL IMAGE

Figure 3. Same target as in figure 2, but with white-Gaussian noise added.
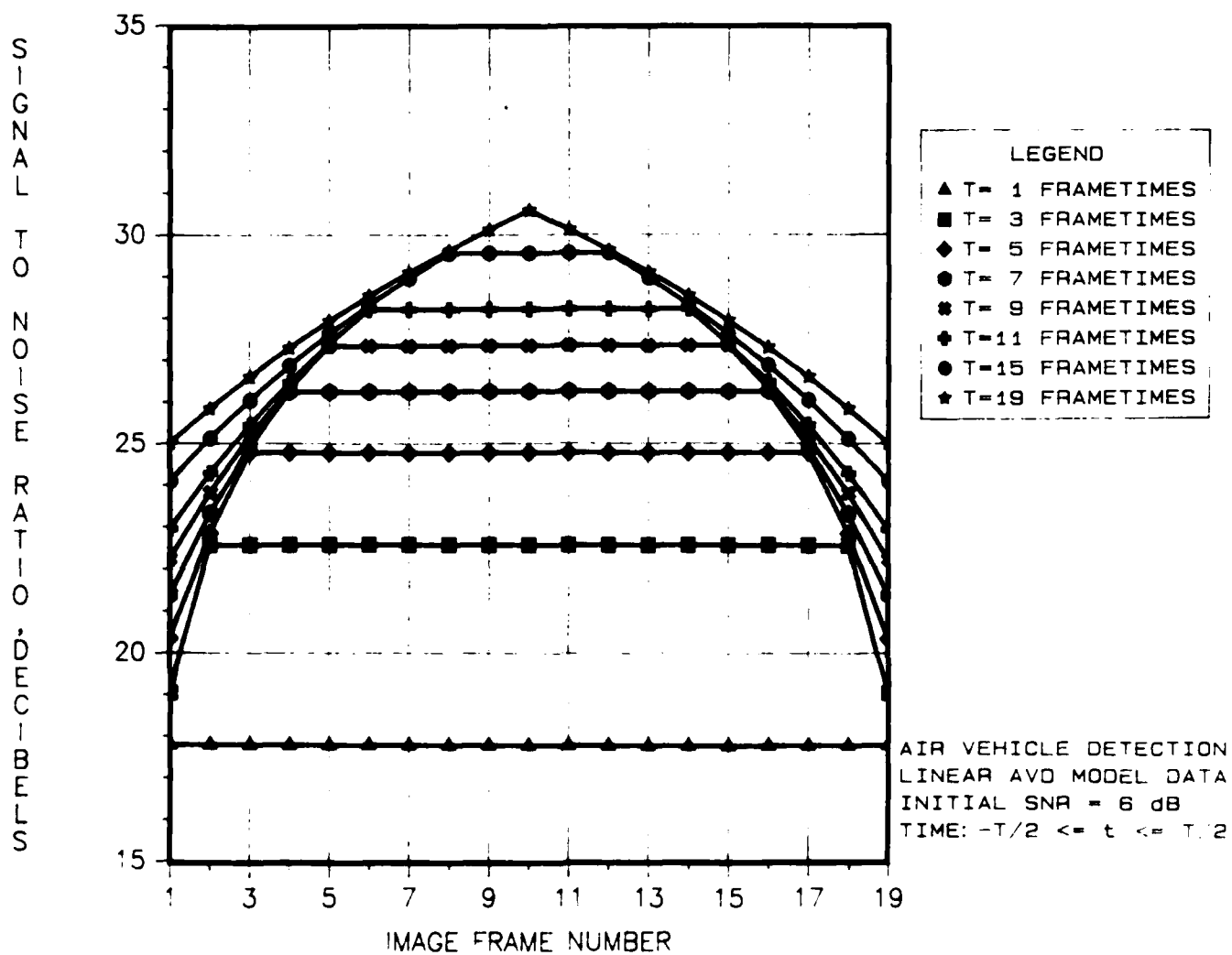
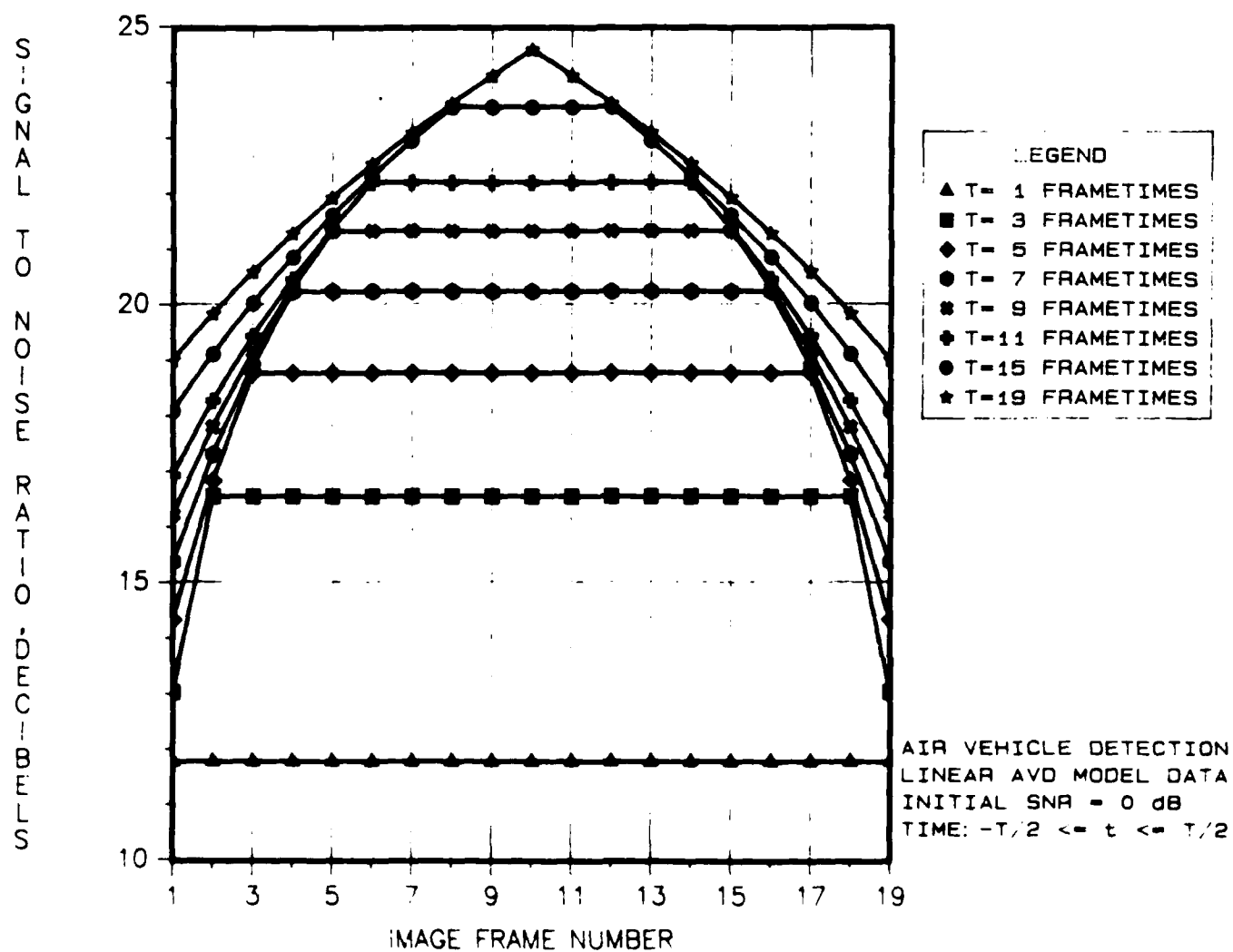Figure 4. Theoretical signal-to-noise ratio from 3-D filtering for SNR = 6 dB

Figure 5 Theoretical signal to-noise ratio from 3-D filtering SNR = 0 dB
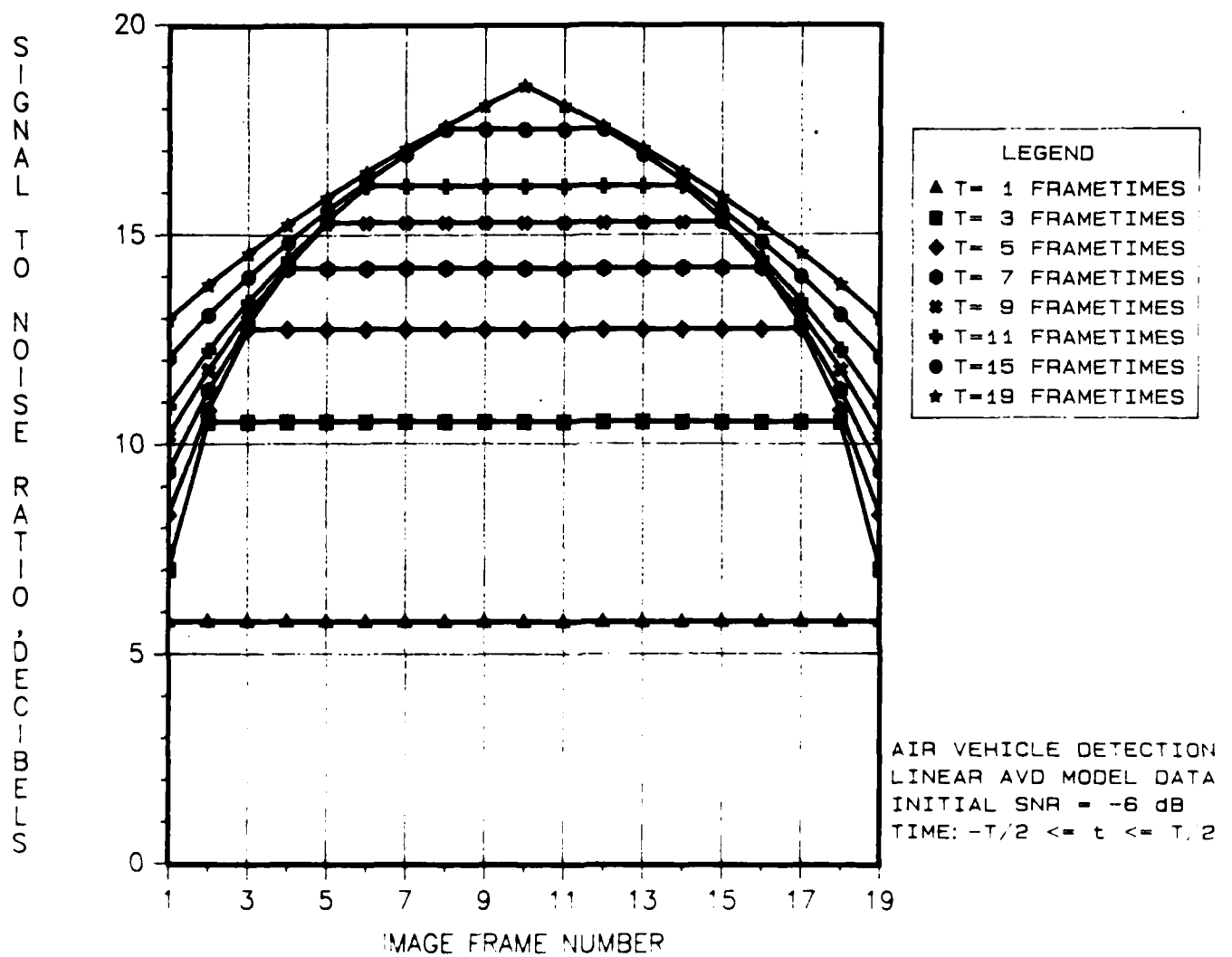
Figure 6. Signal-to-noise ratio from 3-D filtering. SNR = -6 dB

Figures 7 and 8 were typical filtered images obtained by three matched filters processing the image sequences from which figure 6 was taken, using an observation window of 15 frames. These last two figures were created by squaring the real and imaginary parts of each filtered image pixel and storing their individual sum as the resulting filtered pixel for each processed image. The signal-to-noise ratio of each image was calculated by sampling the highest filtered target pixel (the peak created by the matched filtering), calculating the first-order moment of the individual frame (minus the target area contribution), and using the equation

$$SNR_M = \frac{E\{S^2 + N^2\}}{E\{N^2\}} - 1 .$$

(23)

The pixel location of the peak intensity was in row 14 and in a column position equal to the frame number plus two. The signal-to-noise ratios for figure 7 were around 23.5 dB. Specific details of the processed results are as follows.

Figure 8 shows resulting signal-to-noise ratios for the filtered 6-dB image set as a function of the observation window. These signal-to-noise ratios were obtained by averaging 30 samples of measured signal levels and mean noise levels within a $1 \times 10 \times 1 \times 23$ window of each image and using equation 23. It is apparent from this figure that the signal-to-noise ratios for each image increases with integration time, with the greatest gains within the center images. From our discussion in the previous section, this is not too surprising. However, a comparison of figure 8 with figure 4 shows that the measured signal-to-noise ratios have a more graceful falloff from their peak values than theory predicts. The reason for this is shown in figure 9. Recall that figure 1 illustrates the assumed processing geometry for the theoretical development given above. We have an infinite (or very large) number of frames in which a certain number of frames will have a target propagating across the sequence. This allows maximum buildup of signal energy and a constant noise variance to occur. Figure 9 shows the real situation. We are really dealing with a finite number of frames; 19 in this simulation. This implies that the noise variance will be subject to the same energy buildup as the signal energy does, and will be given by

$$VAR\ [y(r,t)] = B(t) \int\!\!\int_{-\infty}^{+\infty} \frac{S_0(r)^2}{N_0}\ d^2r$$

(24)

This is because the ensemble moving-picture processing is a sliding-interval technique and will include zero-filled images in its processing chain for large integration times. The result is a filtered signal-to-noise ratio equal to

$$SNR = B(t) \frac{\int\!\!\int_{-\infty}^{+\infty} \left[\frac{S_0(t)\ [t + t_0 + t] S_0(t)}{N_0}\right]^2}{\int\!\!\int_{-\infty}^{+\infty} \frac{S_0(t)}{N}}$$

(25)

0 dB 3-D MATCHED FILTER RESULT
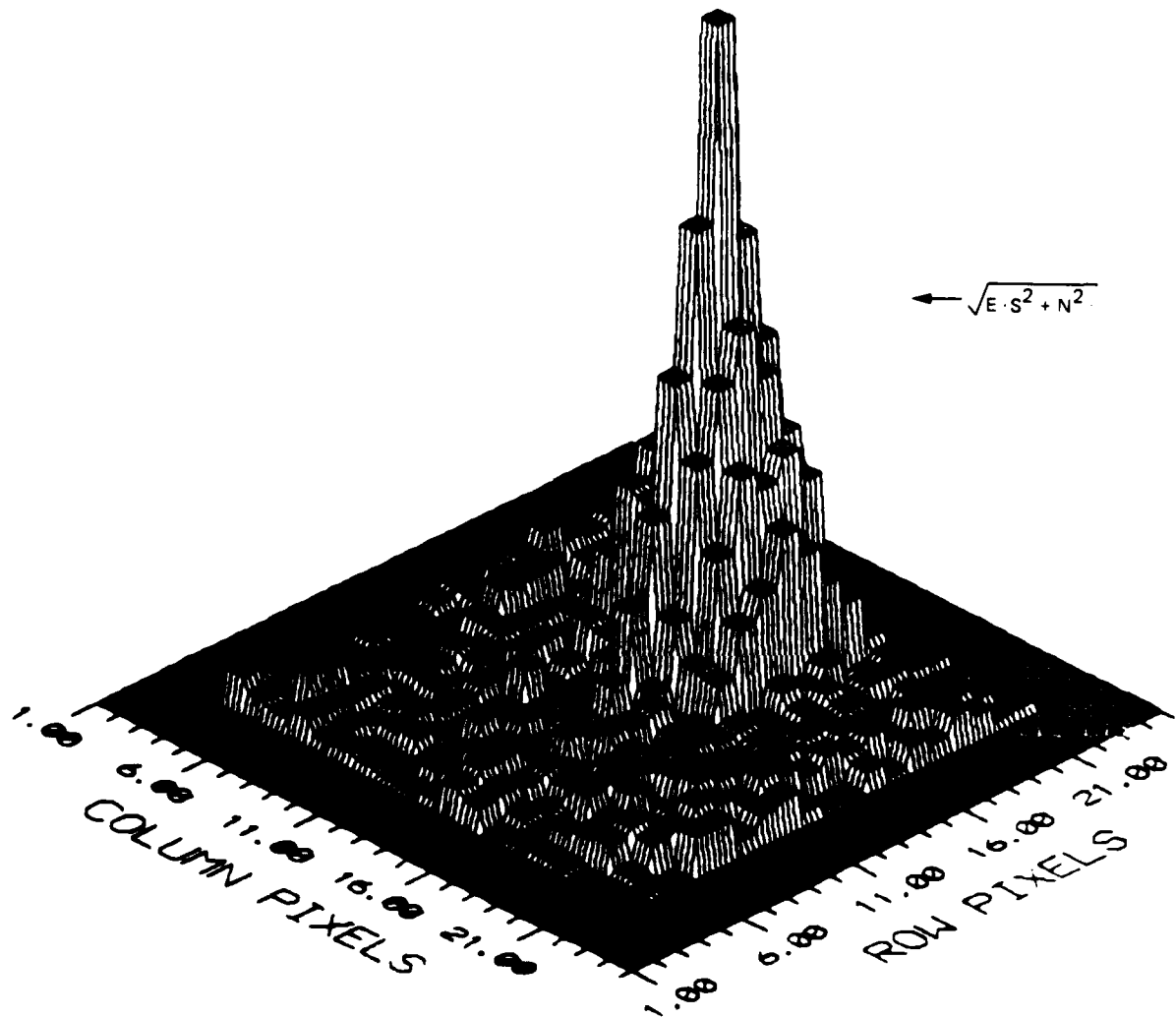

$$\longleftarrow \sqrt{E \cdot S^2 + N^2}$$

Figure 7. Square root of the filtered image sequence frame 8
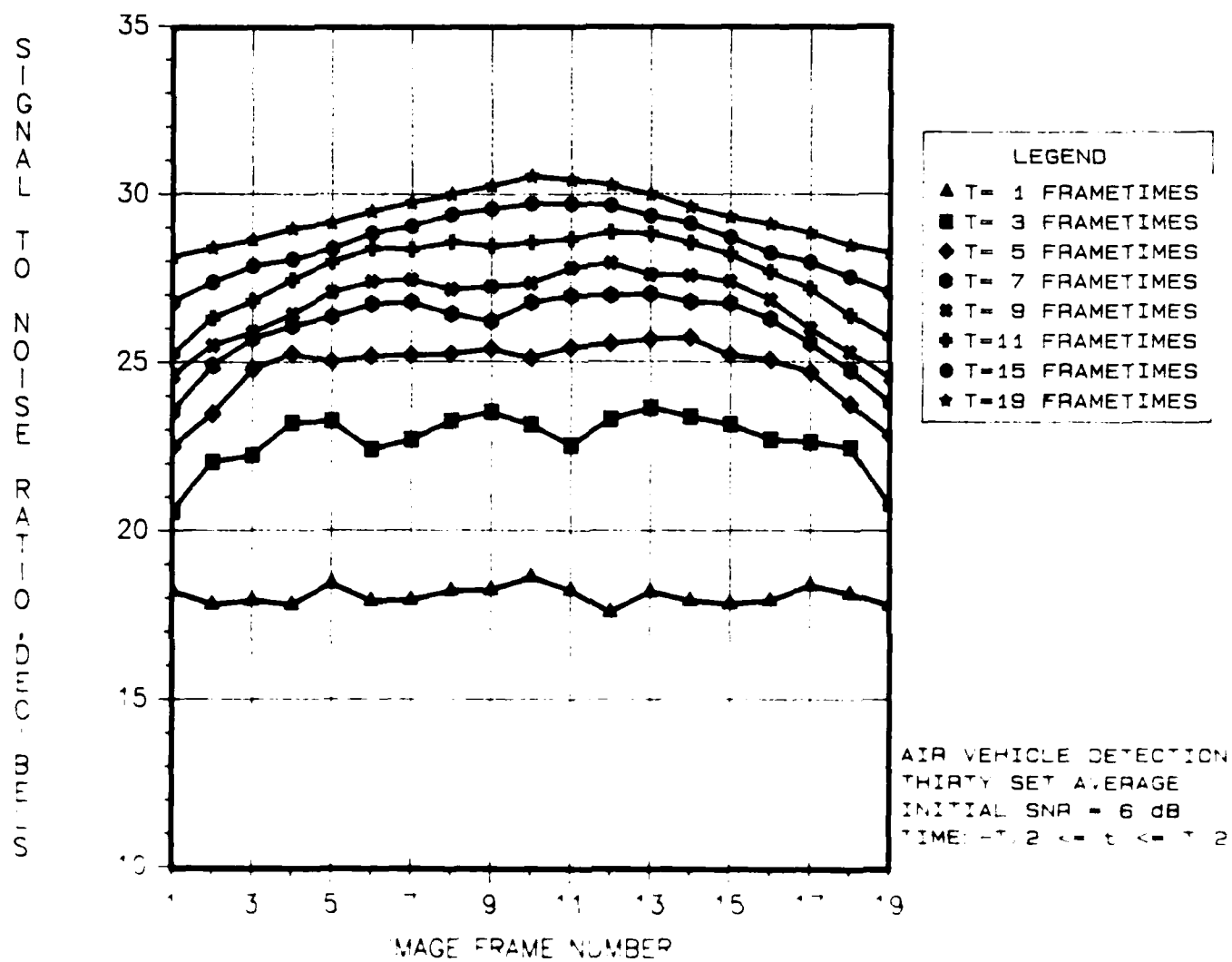
Figure 8. Resulting individual frame signal to noise ratios as a function of frame number for various integration times. SNR = 6 dB

INFINITE DATA SEQUENCE:

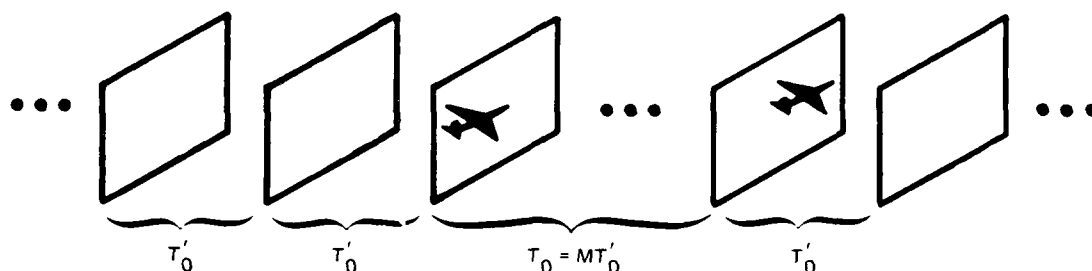$$T_0' \qquad T_0' \qquad T_0 = MT_0' \qquad T_0'$$

Figure 9. Realistic image-processing geometry for three-dimensional matched filtering.

rather than equation 19. Figure 10 shows a comparison of equation 25 with the measured signal-to-noise ratio shown in figure 8. It is apparent that these results agree well with the revised theory. However, it is also clear that there is a slight oscillation, on the order of a dB or less, of the measured signal-to-noise ratio for the smaller filter integration times. Figures 11 and 12 compare equations 12 and 24 with the measured signal and noise variance levels, respectively. It is clear from figure 11 that the measured signal level follows the theory almost perfectly, while figure 12 shows an oscillatory nature in the measured noise variance as compared to theory. This may be a result of our using an infinite-interval processing filter with finite-domain Fourier-transformed imagery, whose effects average out for large filter integration times. However, this oscillatory effect is small and does not negate the power of the technique.

Figure 13 illustrates the measured signal-to-noise ratio from the 0-dB initial SNR simulation with equation 25. As noted earlier, the image sequences used were drawn from a completely different random-number sequence than was used to create the 6-dB set. It is clear that these results also agree well with the revised theory, with the same oscillatory behavior at the lower integration times. Figures 14 and 15 compare equations 12 and 24 with the measured signal and noise variance levels, respectively, and show that the oscillations are in the measured noise variance, as noted before. Figures 16, 17, and 18 repeat the same comparisons as 13, 14, and 15, respectively, except for an initial signal-to-noise ratio of –6 dB. These results are consistent with the other two independent simulations and illustrate that three-dimensional matched filtering can bring a target's presence out of the noise in a predictable fashion. This can be quite important for weak target detection in strong background noise or when target fading occurs.

Figures 10, 13, and 16 indicate that three-dimensional matched filtering creates a matched-filter peak within one frame such that a target no-target decision can be made by means of intensity thresholding there. This suggests that this approach may have merit in a moving-target indicator (MTI) scheme.

4.0 ENSEMBLE MOVING-PICTURE PROCESSING AS A MOVING-TARGET INDICATOR

The sensitivity of ensemble moving-picture processing to velocity mismatch can be assessed as follows. From our development in section 2, it can be seen that a velocity mismatch will only affect the filtered signal level, but not the processed noise level. This implies that one needs only to recalculate the mean signal level $s(r,t)$. The input sequence to

Figure 10. Comparison of revised theoretical signal-to-noise ratio from 3-D filtering with simulated data-processed results. SNR$_i$ = 6 dB.

Figure 11. Comparison of increased signal energy with revised theory: $SNR_i = 6$ dB.

Figure 12. Comparison of filtered image noise variance with revised theory: SNR_i = 6 dB.

Figure 13. Comparison of revised theoretical signal-to-noise ratio from 3-D filtering with simulated data-processed results: SNR$_i$ = 0 dB.

Figure 14. Comparison of measured signal level with procedural results: $SNR_i = 0$ dB.

Figure 15. Comparison of measured noise-level variance with revised theory: $SNR_i = 0$ dB.
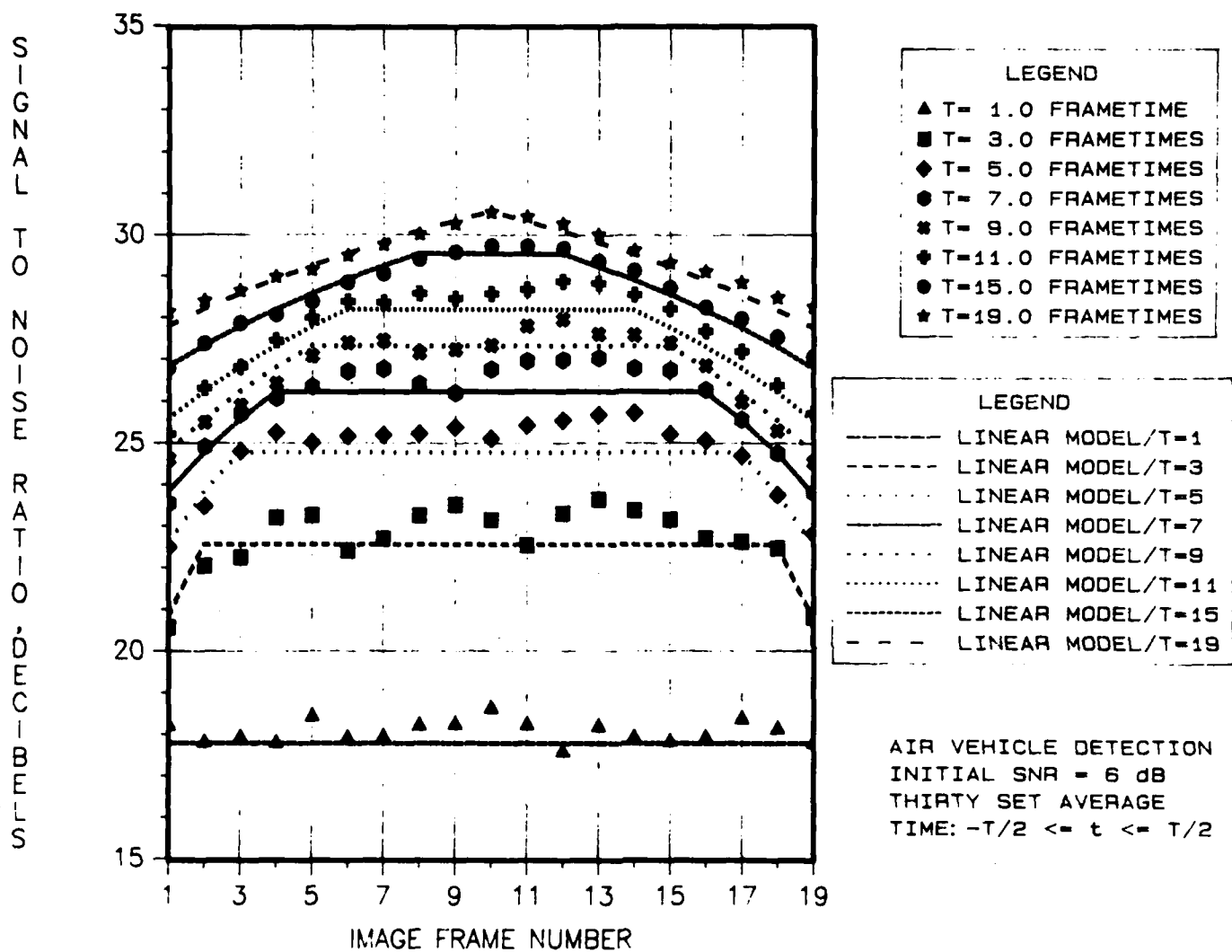
Figure 16. Comparison of revised theoretical signal-to-noise ratio from 3-dB filtering with simulated data-processed results: SNR_i = -6 dB.
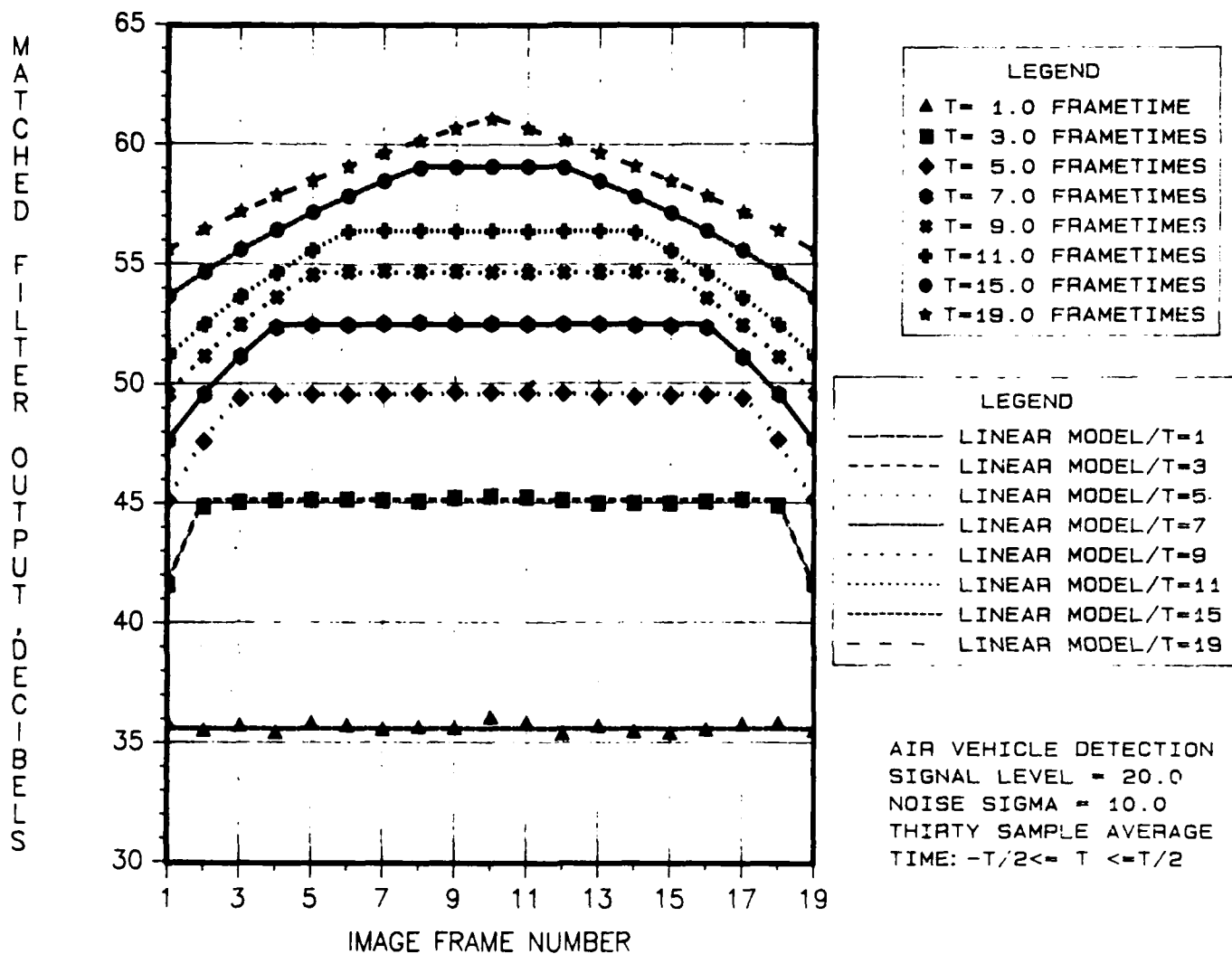
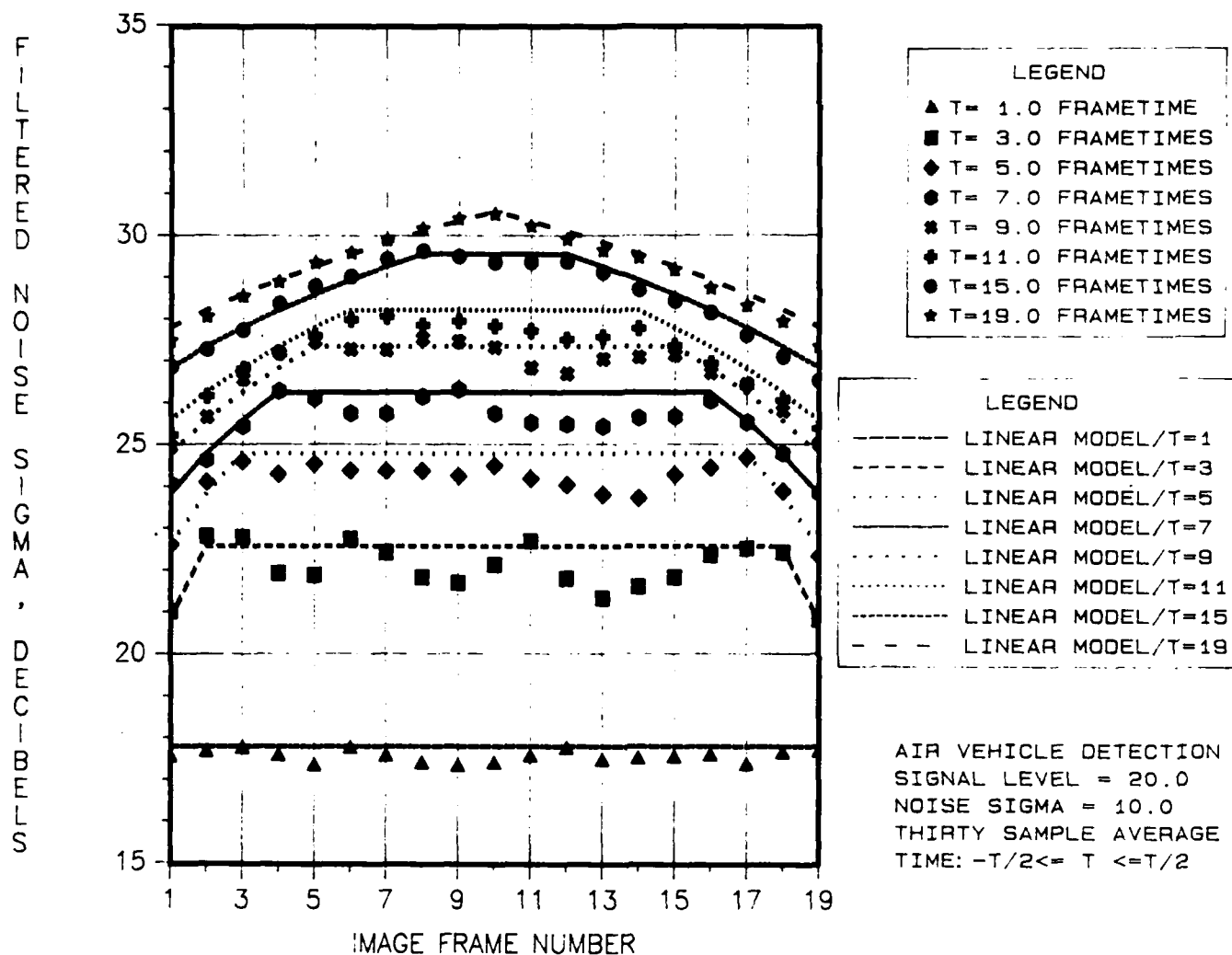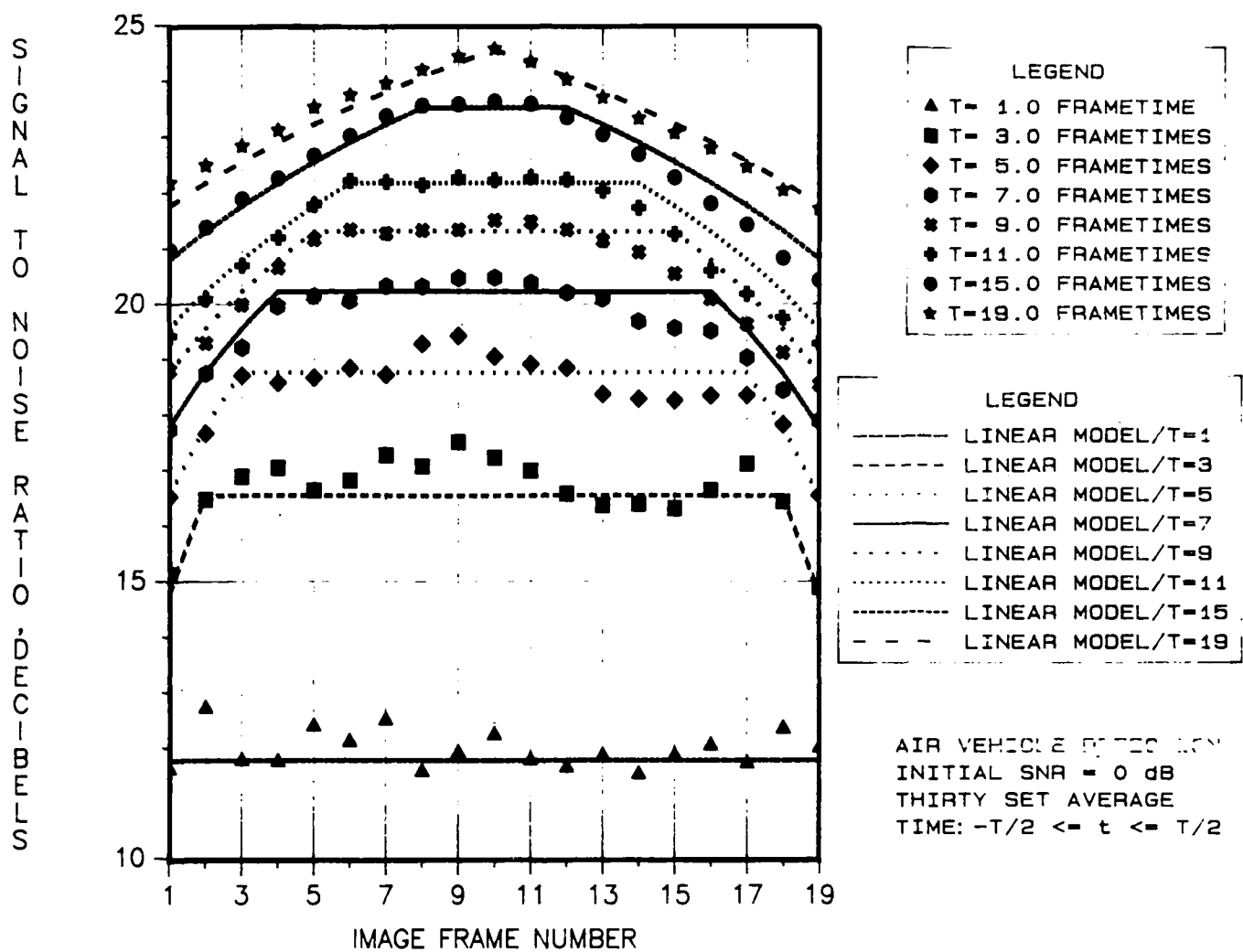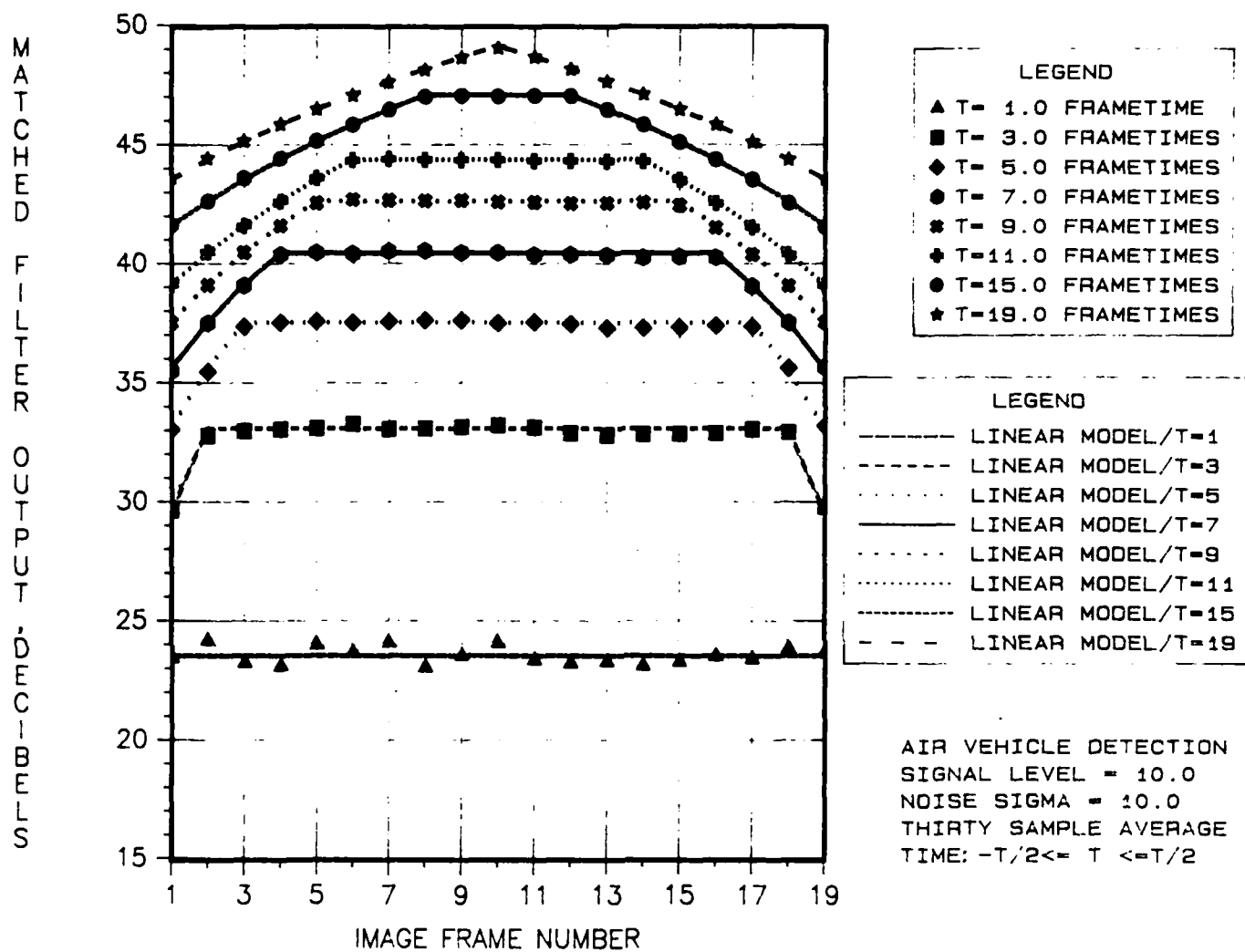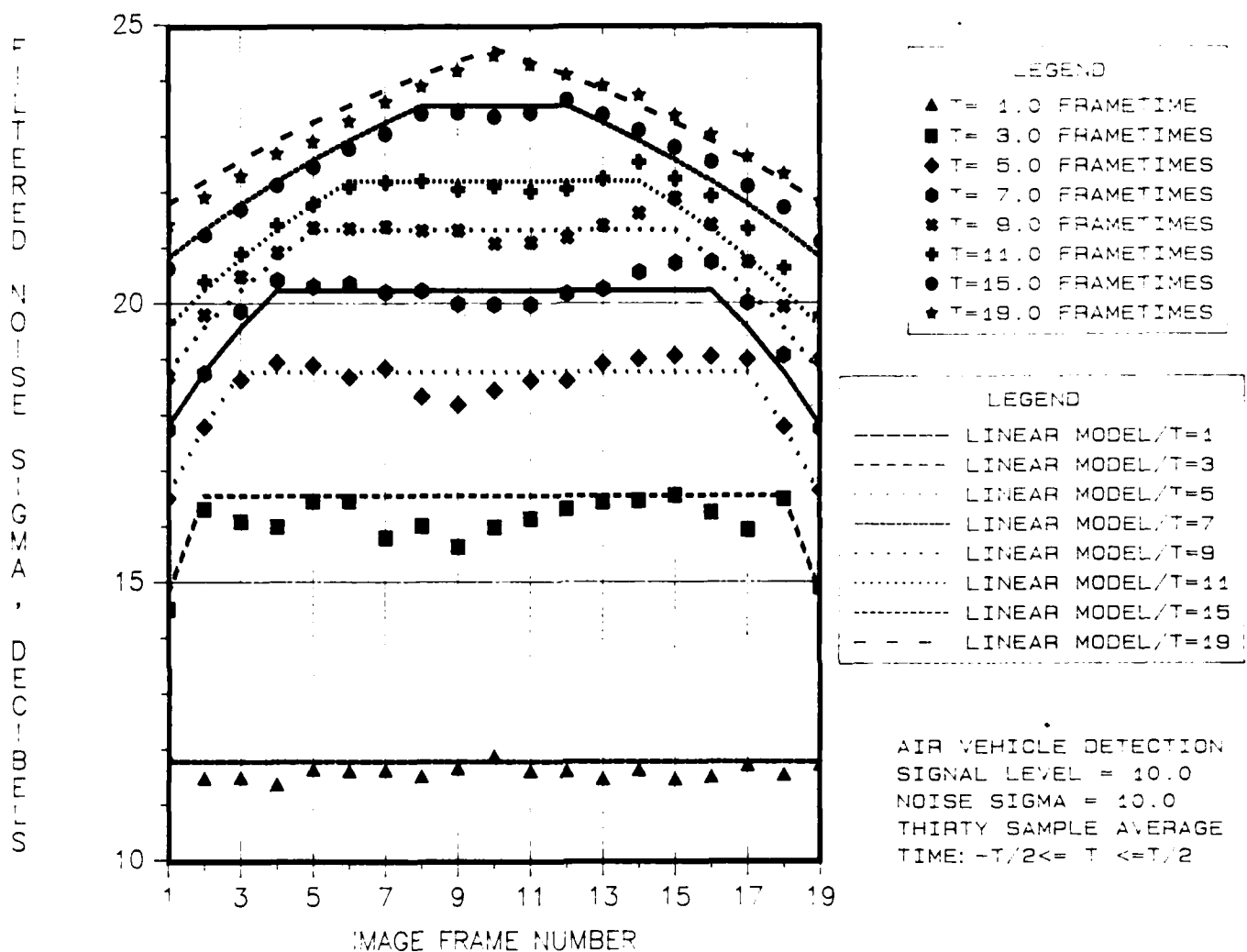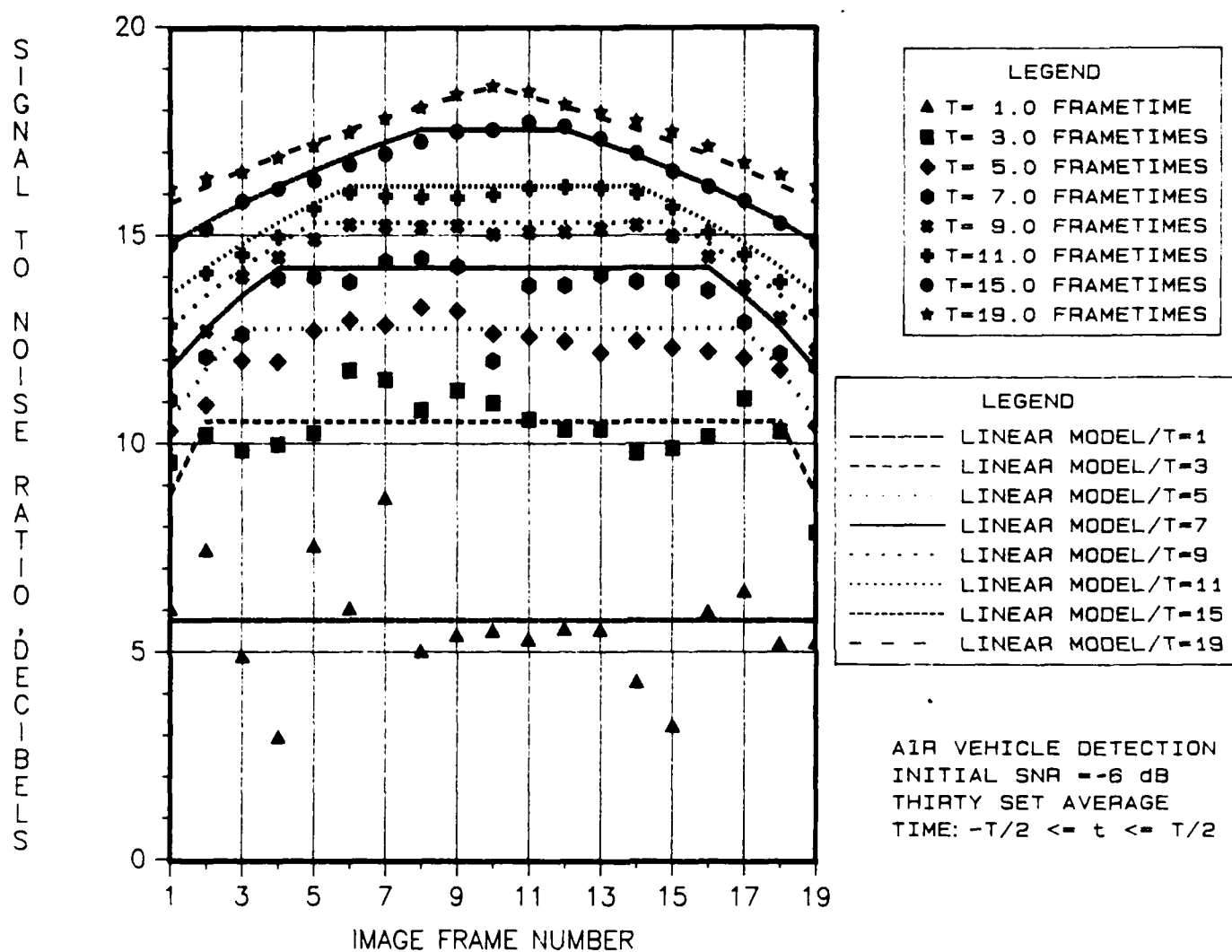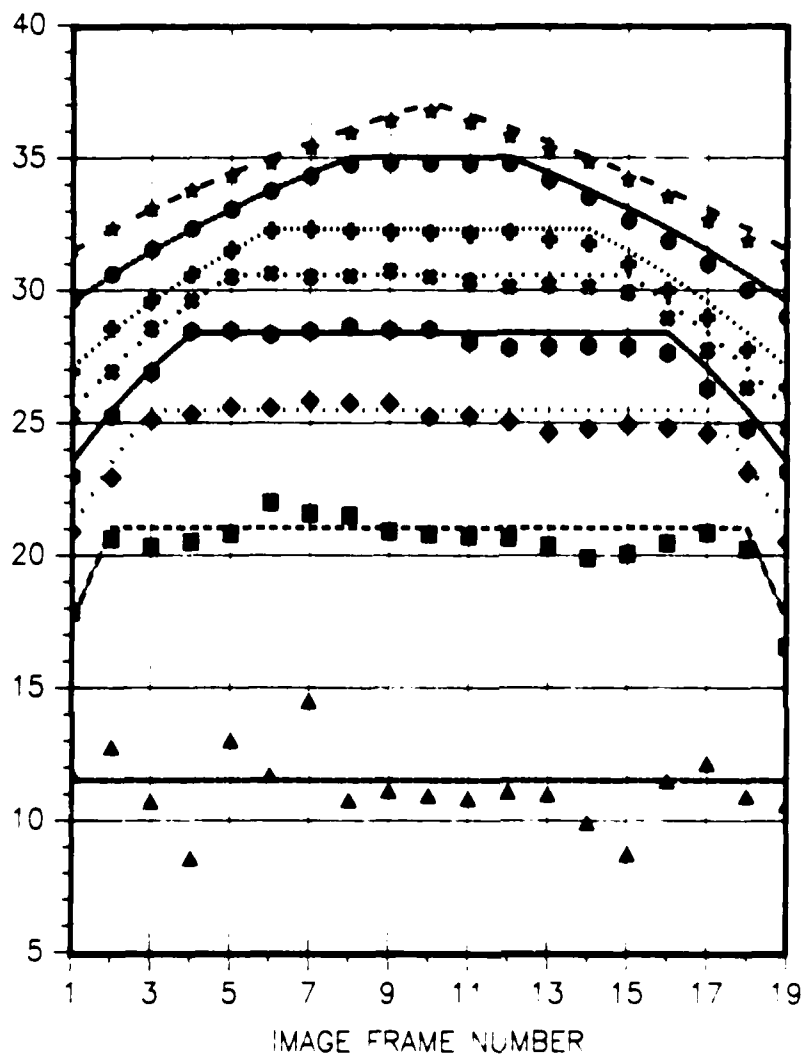Figure 17. Comparison of measured signal energy with revised theory. SNR = -6 dB
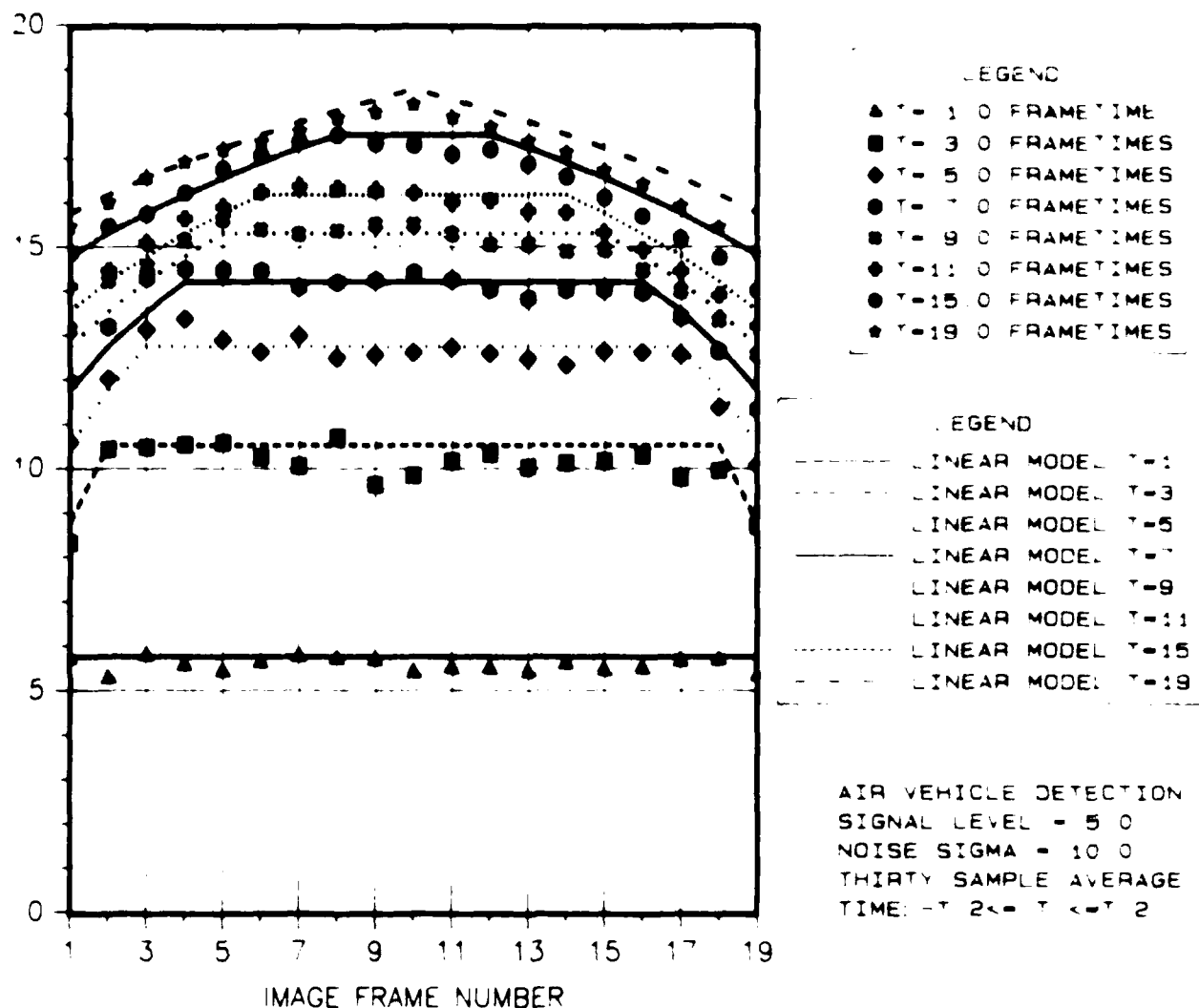
23

Figure 18 Comparison of filtered image noise variance with revised theory, SNR = 6 dB

be processed again is given by equation 7

$$S(x, \omega, t) = I_0 \, \text{sinc}[(\omega + \kappa v_1)t] I_0 \, 2\pi \, \hat{S}_0(k) e^{-\kappa v_0 t}$$

but the processing filter now equals

$$H(x, \omega, t) = [\,\text{sinc}[(\omega + \kappa v_1)t]] \, 2\pi \, \frac{\hat{S}_0^*(k)}{N_0}$$

In the above equations v_0 is the actual target velocity, v_1 is the velocity setting of the filter and S_0 is the Fourier transform of the target's spatial profile in its proper angular orientation. The mean signal level after processing is therefore

$$E[\cdot] =$$

$$\iiint_{-\infty}^{+\infty} \frac{S_0(\cdots + \tau + v_0 t + v_0) t(\cdots - v_0 t) S_0^*(\cdots)}{N_0} \cdots \left[\frac{1}{I_0} \cdots + \frac{1}{1} \cdots \right] d^2 r \, d\tau$$

which goes to

$$E[\cdot] = \iint_{-\infty}^{+\infty} \frac{S_0(\cdots + \tau + v_0 t + v_0 t) S_0^*(\cdots)}{N_0} \, d^2 r$$

for $v_0 = v_1$. Equation 28 shows that the resulting signal level for a velocity mismatch reduces the inherent spatial matched-filter gain by a time-dependent spatial shift proportional to the velocity difference, $v_1 - v_0$. The sensitivity of this mismatch is both a function of target shape as well as velocity difference. For small targets, this technique would serve as an MTI processor.

To test this hypothesis, the 6-dB image set was processed with a set of matched filters tuned to different target speeds. The propagation direction was assumed to be correct. Any directional mismatches would reduce the filter signal level further, so one might consider this a best-velocity-mismatch scenario. The possible target speeds were varied from 0.0 to 3.0 pixels per frame (p/f). The 6-dB target traversing the input frame set was moving at a constant velocity of 1 pixel per frame. Figure 19 shows the measured signal-to-noise ratio at the SNR peak locations used to create figure 10 as a function of airplane speed. The filter observation time is 19. It is apparent that ensemble processing with incorrectly tuned matched filters yields lower signal-to-noise ratios than those resulting from the use of the correct filter, as expected. Interestingly, there is a notable asymmetry between the processed SNRs, depending on whether the filter velocity is above or below the actual target velocity. Specifically, the resulting signal-to-noise ratios degrade slightly more slowly for those filters whose speeds are in excess of the actual speed of 1 p/f. This is more clearly seen in figure 20, which depicts the SNR for the peak frame location, frame 10. From equation 28, we see that a target filter mismatch will result in spatial matched-filter convolution at a nonoptimum offset and at a peak-time-convolution location. In essence, it appears that the resulting filtered target signature is essentially optical blurring of the expected "matched" filter peak in the target movement location. That is, the filter can coherently stack target energy, but in an ambiguous way. This creates

S
I
G
N
A
L

35

30

T
O

N
O
I
S
E

25

R
A
T
I
O

20

O

D
B
S

15

AIR VEHICLE DETECTION
THIRTY SET AVERAGE
INITIAL SNR = 6 dB
TIME -T 2 <= t <= T 2

10

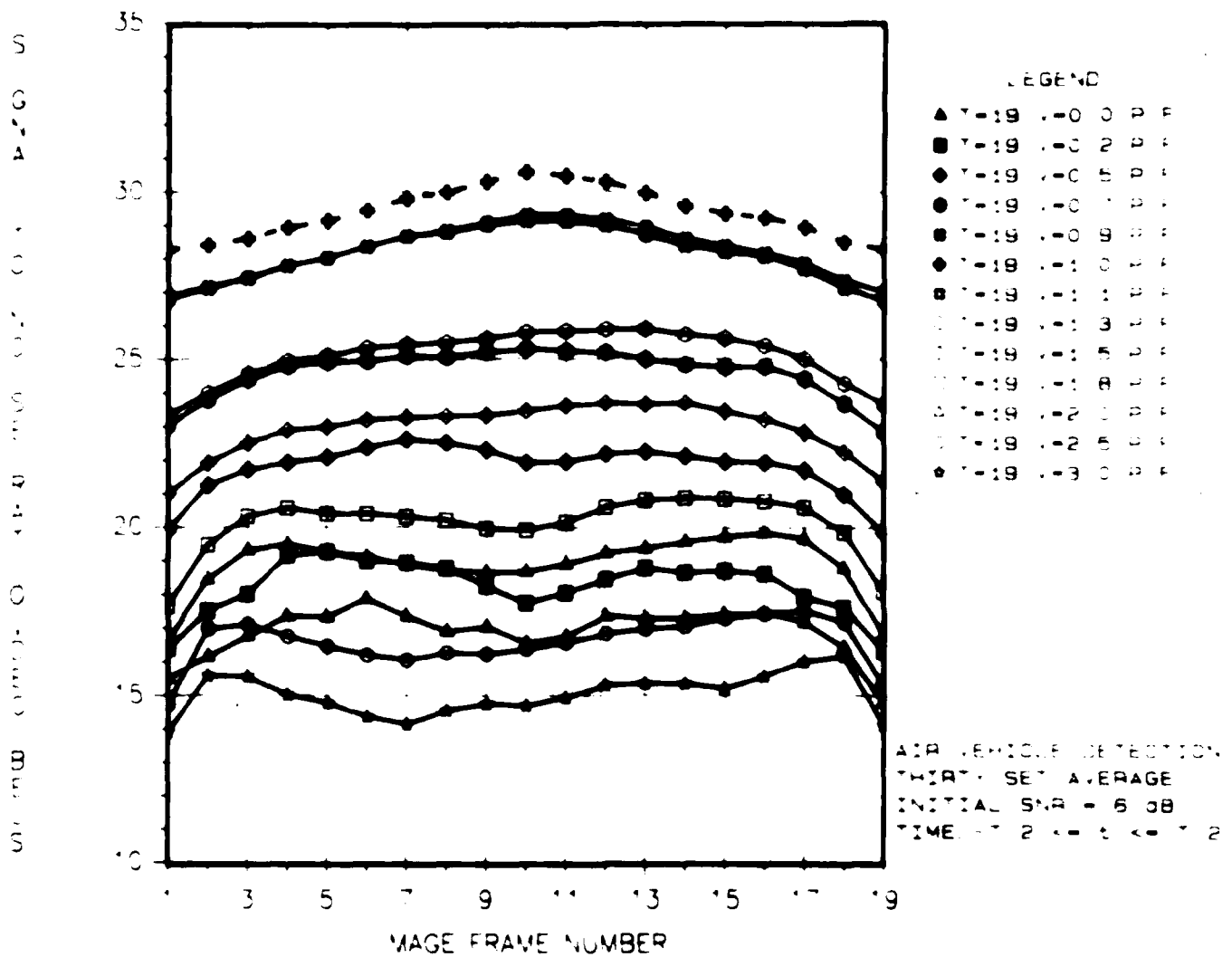3   5   7   9   11   13   15   17   19

IMAGE FRAME NUMBER

Figure 19   Measured signal to noise ratio for various velocity sundential letters as a function of image frame number
T = 19 and SNR = -6 dB

Figure 20   Measured signal to noise ratio at frame 10 for various identity functions

...uncertainty region for the relative location of the target because of the speed mis...
...will have a slight variation in shape and intensity for equal speed diff...
...owing to the symmetry of the target. However, the major reason for the SNR
...is that the mismatched speed filters draw in zero-filled imagery or more nois...
...into the filtering operation. The low-speed filters produced a 1-dB or less increas...
...optimum noise variance over the range used, and this can be attributed to having a
...effective noise filter of lower design speed. The higher speed filters produce... ...
...creased noise variance by drawing zero-filled imagery into the processed result.
...estimates that the nonoptimum SNRs are still well below that of the peak signal-to-
...and the filtering process appears to act as an MTI processor, as suggested above. This
...shown in figure 20 for the location of the peak SNR after matched filtering of...
...In addition, the graceful degradation of the process under small target filter speed
...suggests that a reasonable number of filters may only be required for the MTI
...bank, not an infinite number tuned to all orientations and speeds. This point is
...further illustrated in figures 21 and 22.

Figure 21 gives the measured signal-to-noise ratio at the peak SNR pixel locations...
...create figures 9 and 18, as a function of frame number and various velocity
mismatches. Here we have varied track direction, but have kept target speed at ...p... The
...integration time of the filter is 19, and the angles assessed were 0, +5, +10, +20, +30,
+45, and +60 degrees. This figure illustrates an unusual asymmetry in the filtered output
...for large angle offsets. This is not a target signature related phenomenon, but
...is the contamination of the statistics window by the optical blurring of the filtered
signature profile. This results in an increased noise variance. For example, the filter tuned
...positive 60-degree offset tracks looks for a target traversing the image sequence from left
...right in the downward direction. The resulting filtered image has target energy smeared
...over a broader area because of the filter-target-track mismatch. However, this matched
...filter peak is still somewhat large in magnitude, although large in spatial extent. This is the
...representation of 3-D matched filtering being able to extract partial tracks. In this case
...of the anticipated filter and real target tracks. On the other hand, this partial track
...places target as well as noise energy in the statistic window to a varying degree
...as a function of frame number relative to the filter orientation. Specifically, a 9-dB nois...
...is created in frame 1, decreasing to 3 dB at frame 10 and decaying to zero after that
...60-degree filter creates noise contamination in the opposite sequence order. This
...highlights the uncertainty regime of target location and direction. The filter peak...
...actually oscillates about the true direction of target movement as one progress...
...through a frame set. The optical smear occurs in the opposite direction of the offset and
...that direction increases with offset error. Recognizing this effect, the potential of
3-D filtering as an MTI method can be investigated by using these data. Focusing in on this
...result, the measured signal-to-noise ratio degrades slowly for small angle
mismatches and decreases more rapidly as the track angle offset increases. This is se...
...in figure 22, where the measured SNR in frame 10 is shown as a funct...
...track offset. Again, it is apparent that the filter performance is highly desirable
...MTI point of view. The figure illustrates once again that this filtering technique pick...
partial tracks of those trajectories which overlap. In addition, figure 22 demonstrates
...again that the three-dimensional matched-filtering technique can pick up partial
...which overlap. The reason is that normal matched filtering is primarily
...dependent on the energy of the target than on its detailed shape. For example
...a shaped object correlated with an image of a certain target...
...of final outputs similar to that created by a matched circular filter. It
...that a filter bank can be reduced in size if the mismatch can be tolerated.
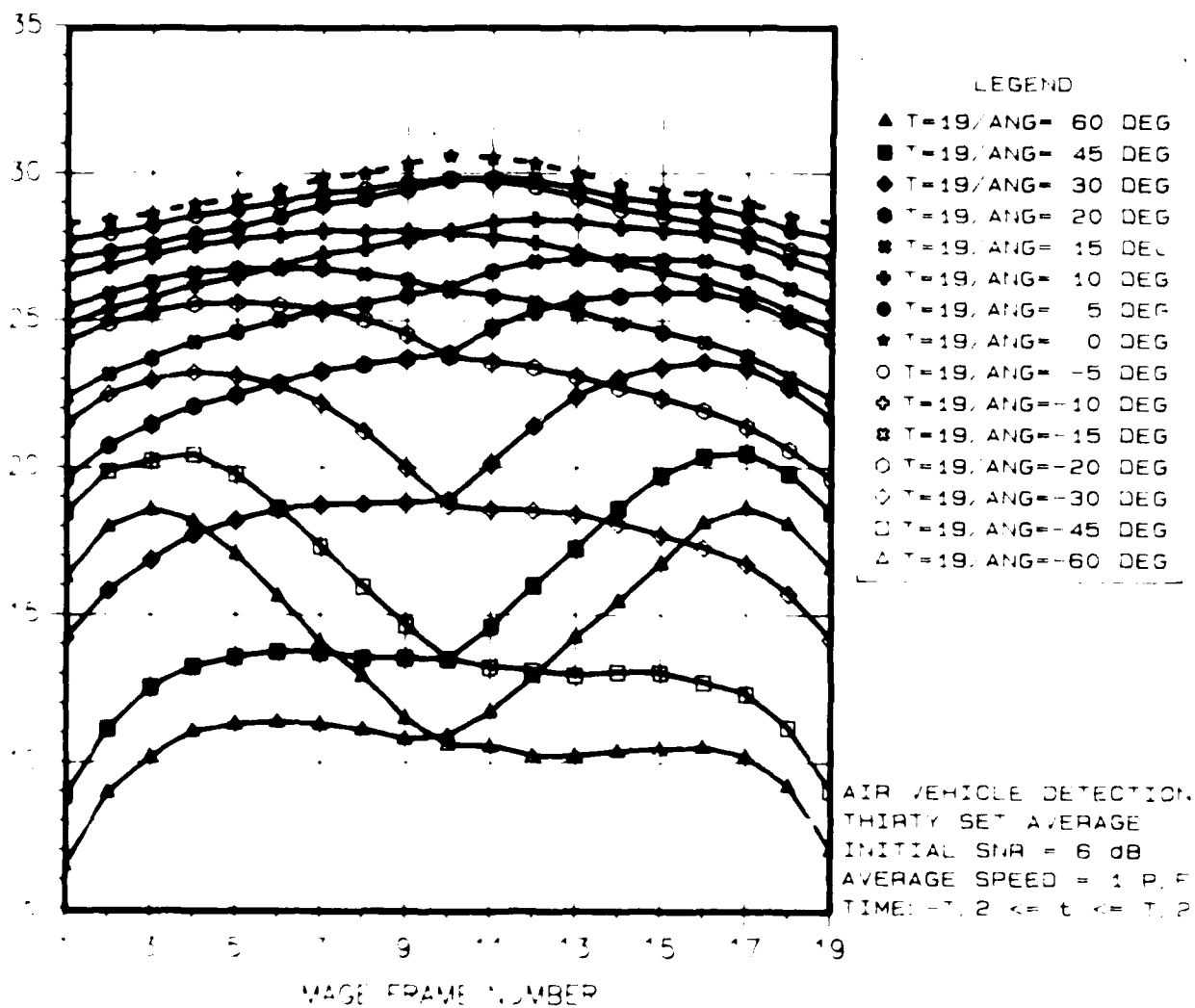
Figure 21 Measured signal to noise ratio for various track angle offsets as a function of image frame number T = 19 and SNR = 6 dB
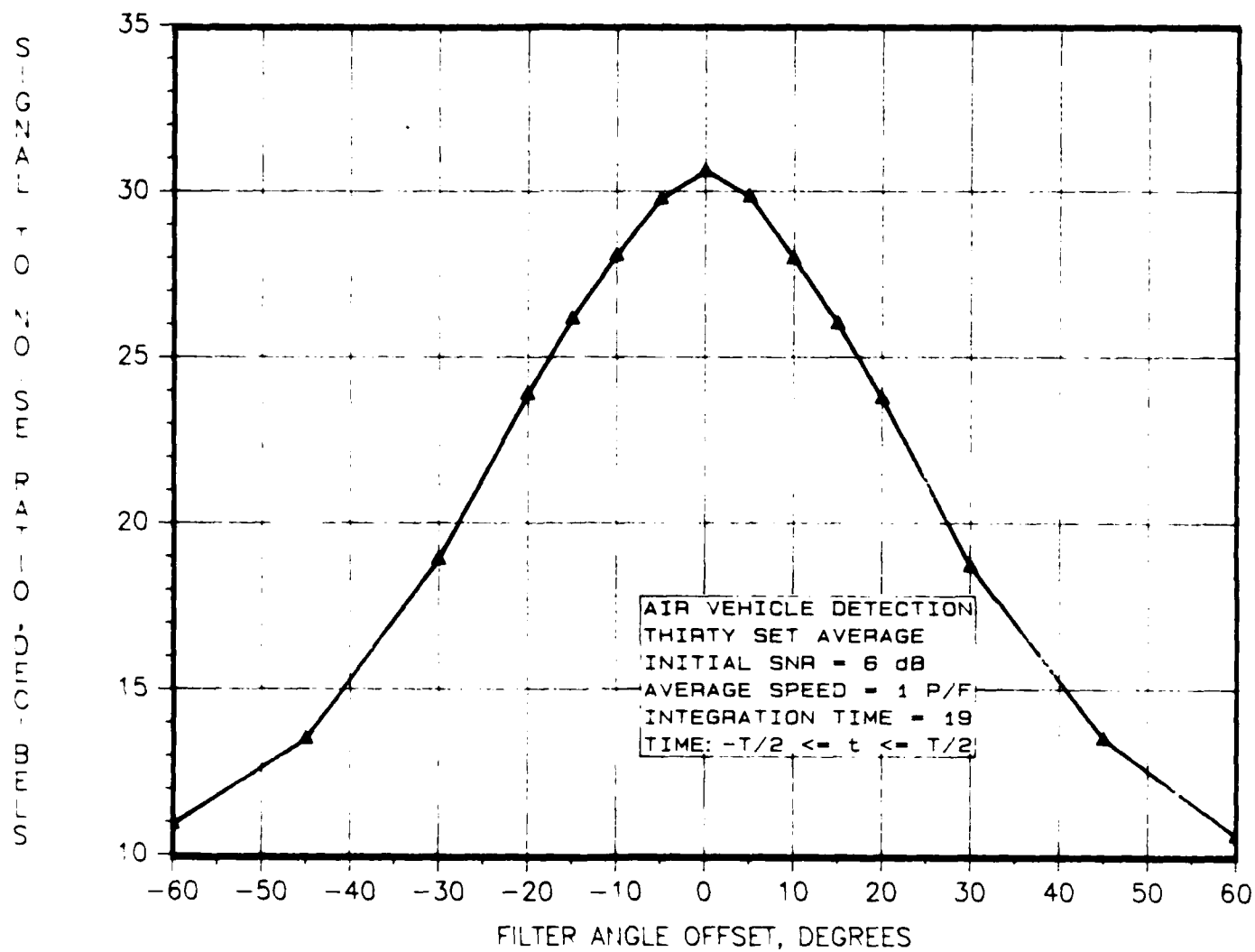
Figure 22. Measured signal-to-noise ratio at frame 10 for various track angle offsets: $T_1 = 19$ and $SNR_i = 6$ dB.

quite desirable from a data-processing point of view and will be investigated further. If true, this means that 3-D filtering for moving-target detection could be viewed as a coarse MTI approach and could hand off potential target information to other systems designed for finer target localization. Otherwise, a derivative matched filter must be used to enhance shape discrimination, assuming that the imagery is adequately sampled [14].

5.0 CONCLUSIONS

In this report, we have shown that the three-dimensional filtering techniques developed by Reed, et al. [12], can be easily modified to act as a space-shift, time-delay-and-integrate matched-filtering technique. Computer simulations verified the validity of this modification. The results demonstrate signal-to-noise ratio gains asymptotically growing by the filter integration time over those normally obtained by two-dimensional matched filtering of the individual frames in a sequence. The specific form of the output is ideally suited for MTI applications, or can be used in conjunction with some other target-speed and detection-localizing algorithm.

6.0 REFERENCES

1. Rosenfeld, A., and A. C. Kak, Digital Picture Processing, second edition, Academic Press, New York, vol 1 and 2, 1982.

2. Moik, J. G., Digital Processing of Remotely Sensed Images, NASA SP-431, National Aeronautics and Space Administration, Washington, DC, 1980.

3. Picture Processing and Digital Filtering, T. S. Huang, editor: Topics in Applied Physics Series, vol 6, Springer-Verlag, New York, 1979.

4. Applications of Digital Signal Processing, A. V. Oppenheim, editor; Prentice-Hall, New York, 1978, chapter 4.

5. Andrews, H. C., and B. R. Hunt, Digital Image Restoration, Prentice-Hall, New York, 1977.

6. Jerlov, N. G., and E. S. Nielsen, Optical Aspects of Oceanography, Academic Press, New York, 1974.

7. Patterson, T. J., D. M. Chabries, and R. W. Christiansen, Image processing for target detection using data from a staring mosaic IR sensor in geosynchronous orbit, Proceedings of the Society of Photographic and Instrumentation Engineers: Applications of Digital Image Processing VII, SPIE vol 504, pp 251-258, 1984.

8. Rausch, H. E., W. I. Futterman, and D. B. Kemmer, Background suppression and tracking with a staring mosaic sensor, Optical Engineering, pp 103-110, Jan-Feb 1981.

9. Rausch, H. E., and J. J. Kohfeld, System design for a staring mosaic sensor, Proceedings of the Society of Photographic and Instrumentation Engineers: Infrared Imaging Technology, SPIE vol 226, pp 53-60, 1980.

10. Mohanty, N. C., Computer tracking of moving point targets, IEEE Transactions on Pattern Analysis and Machine Intelligence, vol PAMI-3, no. 5, pp 606-611, 1981.

11. Barniv, Y., Dynamic Programming Solution for Detecting Dim Moving Targets, IEEE Transactions on Aerospace and Electronic Systems, vol AES-21, no 1, pp 144-156, 1 Jan 1985.

12. Reed, I. S., R. M. Gagliardi, and H. M. Shao, Applications of Three-Dimensional Filtering to Moving Target Detection, IEEE Transactions on Aerospace and Electronic Systems, vol AES-19, no 6, pp 898-905, Nov 1983.

13. Dillard, G. M., Generating random numbers having probability distributions occurring in signal detection problems, IEEE Transactions on Information Theory, vol IT-13, no 4, pp 616-617, 4 Oct 1967.

14. Pratt, W. K., Digital Image Processing, John Wiley and Sons, New York, chapter 14, pp 553-558, 1978.

15. Goodman, J. W., Introduction to Fourier Optics, McGraw Hill, New York, chapter 6, pp 101-140, 1968.

APPENDIX: DERIVATION OF OPTIMUM 3-D MATCHED FILTER FOR COLORED GAUSSIAN NOISE

Consider the remote sensing geometry illustrated in figure A-1. An optical imaging system is located a distance R above a natural terrain with temporal-spatial intensity distribution $n_0'(r;t)$. The resultant imagery generated by this system is sampled by a high-density, high-speed photodiode array and stored in the form of quasicontinuous (both in space and time) image sequences. For incoherent background illumination, the stored intensity distribution $n_0(r;t)$ can be shown to be given by

$$n_0(r;t) = \kappa \int\int_{-\infty}^{+\infty} |h(r - r')|^2 \, n_0'(r;t) \, d^2r' \tag{A-1}$$

where κ is a real constant [15]. In this equation, $h(r)$ is the impulse response function of the optical imaging system under coherent light illumination. The magnitude squared of this function is called the point-spread function (abbreviated PSF), and is linked to the optical-transfer function (OTF) of the imaging system through the relation

$$\mathcal{H}(k) = \frac{\int\int_{-\infty}^{+\infty} |h(r)|^2 \exp\{-ik \cdot r\} \, d^2r}{\int\int_{-\infty}^{+\infty} |h(r')|^2 \, d^2r'} \tag{A-2}$$

If a target of interest moves through the imaged scene, its intensity distribution is also mapped onto the photodiode array. In particular, the target or signal intensity has the form

$$s(r;t) \approx \kappa \int\int_{-\infty}^{+\infty} |h(r - r')|^2 \, s'(r';t) \, d^2r'$$

where s' and s are the intensity distributions of the moving target before and after sampling, respectively. For this discussion, let us assume that n_0 and s are transferred into storage without any additional noise contamination. This implies that the two possible output image sequences are

$$y(r;t) = n_0(r;t) \tag{A-3a}$$

and

$$y(r;t) = n_0(r;t) + s(r;t) \tag{A-3b}$$
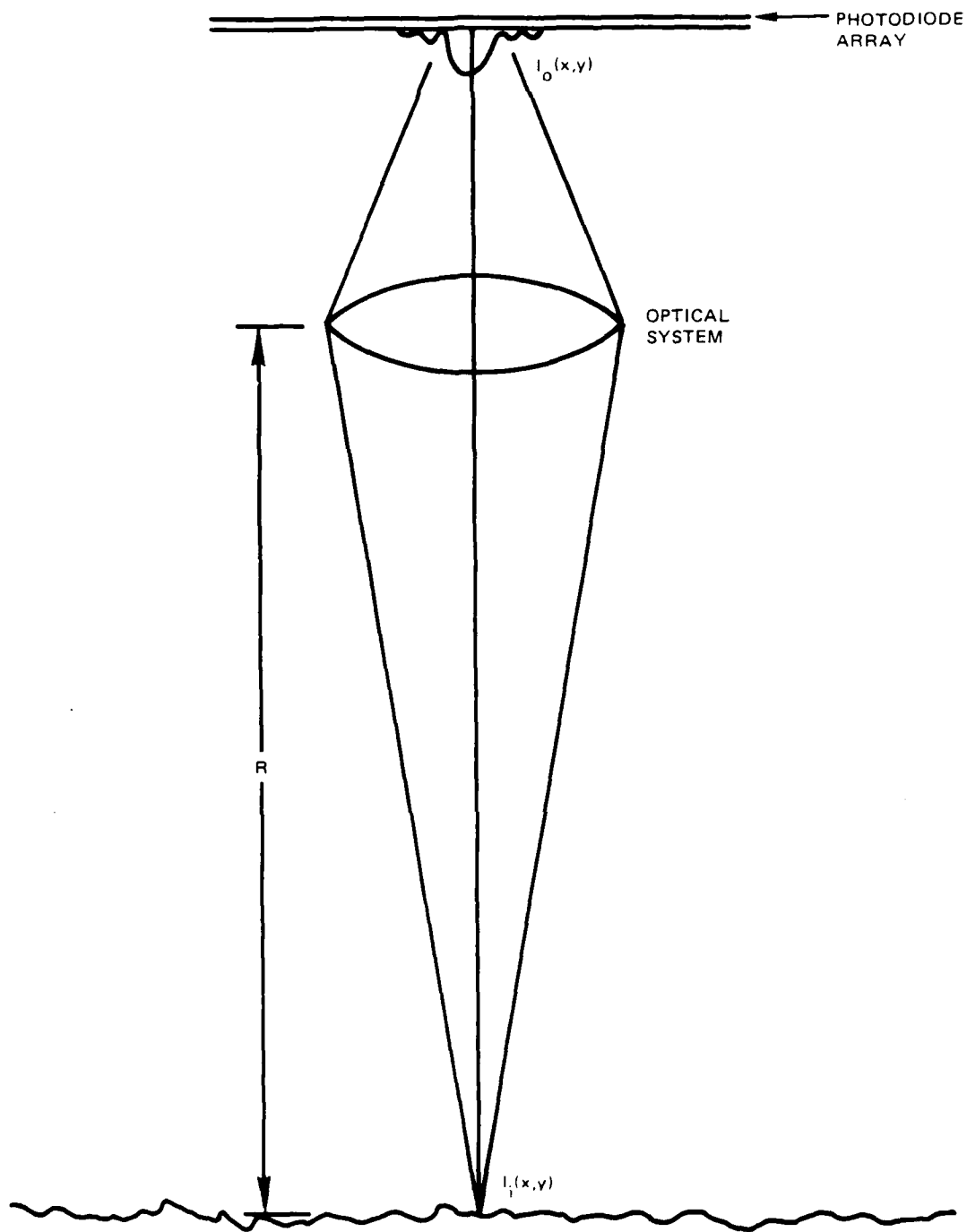
Figure A-1. Optical remote sensing geometry.

with the particular form of $y(r;t)$ depending on whether the target is absent or present, respectively. It is apparent from equation A3-b that the assumed target of interest is transparent to the background illumination, is blurred to the point that this additive relation approximately holds, is small compared to the pixel area, or is contained in frame-to-frame difference data. Although these assumptions may not include all possible remote-sensing scenarios, the application of maximum-likelihood detection techniques to three-dimensional image processing may still prove useful in target-localization situations not covered by equation A-3b.

Given the above, Reed, et al. [12], developed the optimum three-dimensional match filter for moving-target detection shown in figure A-2, and which can be described as follows: The target of interest is specified to possess a spatial profile $s_0(r)$ and a temporal intensity function $a(t)$. In addition, it traverses the imaged terrain at a velocity v. This gives a stored-target intensity distribution of the form

Figure A-2. 3-D matched-filter processing procedure.

$$s(\underline{r};t) \approx \kappa \, a(t) \int\!\!\int_{-\infty}^{+\infty} |h(\underline{r} - \underline{r}')|^2 \, s_0(\underline{r}' - \underline{r}_0 - \underline{v}t) \, d^2r' \qquad (A\text{-}4)$$

with $\underline{r}_0$ being the location of the target at $t = 0$. Fourier transforming equation A-4 yields

$$S(\underline{k},\omega) = \int\!\!\int\!\!\int_{-\infty}^{+\infty} s(\underline{r};t) \exp\{-i\underline{k}\cdot\underline{r} - i\omega t\} \, d^2r\,dt$$

$$= \int\!\!\int\!\!\int_{-\infty}^{+\infty} a(t) \int\!\!\int_{-\infty}^{+\infty} s_0(\underline{r}' - \underline{r}_0 - \underline{v}t) \, |h(\underline{r} - \underline{r}')|^2 \exp\{-i\underline{k}\cdot\underline{r} - i\omega t\} \ldots$$

$$= \int\!\!\int\!\!\int_{-\infty}^{+\infty} a(t) \, s_0(\underline{r}'') \int\!\!\int_{-\infty}^{+\infty} |h(\underline{r} - \underline{r}'' - \underline{r}_0 - \underline{v}t)|^2 \exp\{-i\underline{k}\cdot\underline{r}\} \, d^2r \, \exp\{-i\omega t\} \, d^2r''\,dt$$

$$= \int\!\!\int\!\!\int_{-\infty}^{+\infty} a(t) \, s_0(\underline{r}'') \int\!\!\int_{-\infty}^{+\infty} |h(\underline{r}''')|^2 \exp\{-i\underline{k}\cdot(\underline{r}''' + \underline{r}'' + \underline{r}_0 + \underline{v}t)\} \, d^2r'''$$

$$\exp\{-i\omega t\} \, d^2r''\,dt$$

$$= G(\underline{k}) \exp\{-i\underline{k}\cdot\underline{r}_0\} \int\!\!\int_{-\infty}^{+\infty} a(t) \, s_0(\underline{r}'') \exp\{-i\underline{k}\cdot\underline{r}'' - it(\omega + \underline{k}\cdot\underline{v})\} \, d^2r''\,dt$$

$$= \exp\{-i\underline{k}\cdot\underline{r}_0\} \, A(\omega + \underline{k}\cdot\underline{v}) \, S_0(\underline{k}) \, G(\underline{k}) \qquad (A\text{-}6)$$

where

$$A(\omega) = \int\!\!\int_{-\infty}^{+\infty} a(t) \exp(-i\omega t)\, dt \tag{A-7}$$

$$S_0(\underset{\sim}{k}) = \int\!\!\int_{-\infty}^{+\infty} s_0(\underset{\sim}{r}) \exp(-i\underset{\sim}{k}\cdot\underset{\sim}{r})\, d^2r \tag{A-8}$$

$$G(\underset{\sim}{k}) = \int\!\!\int_{-\infty}^{+\infty} |h(\underset{\sim}{r})|^2 \exp(-i\underset{\sim}{k}\cdot\underset{\sim}{r})\, d^2r \tag{A-9}$$

$$= \int\!\!\int_{-\infty}^{+\infty} G_0(\underset{\sim}{k}' - \underset{\sim}{k}) G_0^*(\underset{\sim}{k}')\, d^2k \tag{A-10}$$

and

$$G_0(\underset{\sim}{k}) = \int\!\!\int_{-\infty}^{+\infty} h(\underset{\sim}{r}) \exp(-i\underset{\sim}{k}\cdot\underset{\sim}{r})\, d^2r \quad . \tag{A-11}$$

The noise in the received pictures is given by

$$n_0(\underset{\sim}{r};t) = \int\!\!\int_{-\infty}^{+\infty} n_0'(\underset{\sim}{r} - \underset{\sim}{r}';t) |h(\underset{\sim}{r}')|^2\, d^2r' \quad . \tag{A-12}$$

This implies that the autocorrelation function for the received clutter is equal to

$$\phi_0(\underset{\sim}{r};t) = E\cdot n_0(\underset{\sim}{r}';t') n_0(\underset{\sim}{r}' + \underset{\sim}{r};t')\cdot$$

$$= \int\!\!\int\!\!\int\!\!\int_{-\infty}^{+\infty} |h(\underset{\sim}{r}'')|^2\, E\cdot n_0'(\underset{\sim}{r}' - \underset{\sim}{r}'';t') n_0'(\underset{\sim}{r}' - \underset{\sim}{r}'' + \underset{\sim}{r};t' + t)\cdot |h(\underset{\sim}{r}''')|^2\, d^2r''\, d^2r'''$$

$$= \int\!\!\int\!\!\int\!\!\int_{-\infty}^{+\infty} |h(\underset{\sim}{r}'')|^2\, E\{n_0'(\underset{\sim}{r}';t') n_0'(\underset{\sim}{r}' + \underset{\sim}{r}'' + \underset{\sim}{r} - \underset{\sim}{r}''';t' + t)\}\, |h(\underset{\sim}{r}''')|^2\, d^2r''\, d^2r'''$$

$$= \int\!\!\int\!\!\int\!\!\int_{-\infty}^{+\infty} |h(\underset{\sim}{r}'')|^2\, \phi_0'(\underset{\sim}{r} + \underset{\sim}{r}'' - \underset{\sim}{r}''';t)\, |h(\underset{\sim}{r}''')|^2\, d^2r''\, d^2r''' \tag{A-13}$$

with

$$\phi_0'(\underline{r};t) = E \cdot n_0'(\underline{r}';t') n_0'(\underline{r}' + \underline{r}, t + t')$$

(A-14)

The power spectrum of the received clutter is then

$$\Phi_0(\underline{k};\omega) = \int\!\!\int\!\!\int_{-\infty}^{+\infty} \phi_0(\underline{r};t) \exp[-i\underline{k} \cdot \underline{r} - i\omega t] \, d^2r \, dt$$

$$= \int\!\!\int\!\!\int\!\!\int\!\!\int\!\!\int\!\!\int\!\!\int_{-\infty}^{+\infty} |h(\underline{r}'')|^2 \phi_0'(\underline{r} + \underline{r}'' - \underline{r}''', t) |h(\underline{r}''')|^2$$

$$\exp[-i\underline{k} \cdot \underline{r} - i\omega t] \, d^2r'' \, d^2r''' \, d^2r \, dt$$

(A-15)

$$= \Phi_0'(\underline{k};\omega) \int\!\!\int\!\!\int\!\!\int_{-\infty}^{+\infty} |h(\underline{r}'')|^2 |h(\underline{r}''')|^2 \exp[-i\underline{k} \cdot (\underline{r}''' - \underline{r}'')] \, d^2r'' \, d^2r'''$$

$$= \Phi_0'(\underline{k};\omega) G(\underline{k}) G(-\underline{k})$$

$$= \Phi_0'(\underline{k};\omega) |G(\underline{k})|^2$$

(A-16)

where

$$\Phi_0'(\underline{k};\omega) = \int\!\!\int\!\!\int_{-\infty}^{+\infty} \phi_0'(\underline{r};t) \exp[-i\underline{k} \cdot \underline{r} - i\omega t] \, d^2r \, dt$$

(A-17)

and

$$G^*(\underline{k}) = G(-\underline{k}) \ .$$

(A-18)

The optimum matched filter for optical target detection is easily shown to be

$$H(\underline{k};\omega) = \frac{S^*(\underline{k};\omega)}{\Phi_0(\underline{k};\omega)}$$

(A-19)

by maximizing the received signal-to-noise ratio

$$SNR = \frac{(E\{y(\underline{r};t)\})^2}{VAR\{y(\underline{r};t)\}}$$

A-5

...S. chapter 19. Substituting equations X-6 and X-16 into equation X-19 the optimum three-dimensional matched filter for moving targets is thus

$$H(\kappa, \omega) = \frac{V^*(\omega + \kappa \cdot v) S_0^*(\kappa)}{\Phi_{nn}(\kappa, \omega) G(\kappa)} \qquad (A\text{-}20)$$

The term t_0 in equation X-20 is set to zero so that the origin of the output plane becomes the point of no translational offset between the filtered and nonfiltered images.

END

8 - 87

DTIC